nature neuroscience

Article

https://doi.org/10.1038/s41593-025-02157-0

Phosphorylated tau exhibits antimicrobial activity capable of neutralizing herpes simplex virus 1 infectivity in human neurons

Received: 24 July 2024

Accepted: 28 October 2025

Published online: 17 December 2025

Check for updates

William A. Eimer[1,2] ✉, Alex S. Rodriguez[1,2], Michael T. DeFao[1,2], Simon Ehricke[3], Joseph Park[1,2], Deepak K. Vijaya Kumar[1,2], Nanda K. Navalpur Shanmugam[1,2], Sanjana Singh[4], Tara Sawhney[5], Robert D. Moir[1,2] & Rudolph E. Tanzi[1,2] ✉

Tau is a microtubule-associated cytoskeletal protein, which, when hyperphosphorylated and aggregated, can result in a myriad of different tauopathies, including Alzheimer's disease (AD). We previously showed that the principal component of senile plaques, amyloid beta (Aβ), is an antimicrobial peptide capable of binding and entrapping microbial pathogens. Here we show that tau is hyperphosphorylated in neurons in response to viral infection and can neutralize herpes simplex virus 1 (HSV-1) infectivity by directly binding to viral capsids. Our data suggest that the 'pathogenic' characteristics of tau hyperphosphorylation, microtubule destabilization and aggregation are part of an antiviral response, in which tau serves as a host defense protein in the innate immune system of the brain. The combined antimicrobial activities of Aβ and phosphorylated tau resulting in Aβ plaques and neurofibrillary tangles, along with neuroinflammation, suggest that AD neuropathology may have evolved as an orchestrated innate immune host defense response to microbial infection in the brain.

Amyloid beta (Aβ) deposited in senile plaques and hyperphosphorylated tau in neurofibrillary tangles (NFTs) have long been considered to play pathological roles in the etiology and pathogenesis of AD[1]. The presence of abundant levels of amyloid plaques and NFTs are required for a confirmed diagnosis of AD. Tau is a microtubule-associated protein that promotes and coordinates tubulin polymerization into microtubules in neurons[2]. Microtubules are essential for axonal transport between the neuronal synapse and soma. Six different isoforms of tau exist in the human brain, generated by alternative splicing of the tau gene *MAPT* (microtubule-associated protein tau). These isoforms vary by containing three or four microtubule-binding domain repeats (3R or 4R, respectively) and zero to two N-terminal inserts (0N, 1N and 2N), with approximately equal representation of 3R and 4R tau isoforms in adult human brain[3]. Detachment of tau from microtubules, hyperphosphorylation and phosphorylated tau (p-tau) aggregation into NFTs are the defining pathological elements of tauopathies, including AD. Various types of tauopathy are differentiated by the isoform of tau that is prone to pathological aggregation and by the individual driving factors that cause tau to dissociate from microtubules—for example, genetic mutations, increased tau expression, decreased tau clearance and increased kinase activity[4]. Although these characteristics are primarily associated with the pathogenic nature of tau, they also share commonalities with antimicrobial peptides (AMPs)[5–7].

The innate immune system is an evolutionarily conserved, broad-spectrum host defense system comprising epitope-recognizing receptors, small microbial-binding peptides called AMPs and

[1]Genetics and Aging Research Unit, Henry and Allison McCance Center for Brain Health, MassGeneral Institute for Neurodegenerative Disease, Charlestown, MA, USA. [2]Department of Neurology, Massachusetts General Hospital and Harvard Medical School, Charlestown, MA, USA. [3]Ulm University, Ulm, Germany. [4]Harvard University, Cambridge, MA, USA. [5]Wellesley College, Wellesley Hills, MA, USA. ✉e-mail: weimer@mgh.harvard.edu; tanzi@helix.mgh.harvard.edu

phagocytic cells—for example, myeloid cells. AMPs are crucial in the innate immune system's initial response to an infection, in which AMPs directly bind to, entrap and neutralize invading pathogens and occasionally function as a modulator of inflammatory response[8,9]. We and others previously demonstrated that Aβ is an AMP capable of entrapping, killing or neutralizing bacterial, fungal and viral infections in both in vitro and in vivo model systems[10–13]. The antimicrobial protection hypothesis of AD is based on these results, stipulating that Aβ is not an errant catalytic by-product of the Aβ precursor protein (APP), but evolved as a physiologically relevant antimicrobial peptide as part of the innate immune system, particularly in the brain[14].

Tau possesses many well-established characteristics and properties that mirror those of Aβ, raising the prospect that tau may also have a role as an AMP. Tau phosphorylation in AD is induced by Aβ amyloidosis, suggesting that it may play a tertiary role in microbial host defense, especially for pathogens that escape the AMP activity of Aβ[15–18]. This is most evident in the ability of Herpes simplex virus 1 (HSV-1) to bypass extracellular immune networks by retrograde axonal transport along the microtubules, which are stabilized by tau[19,20]. Aggregates of hyperphosphorylated tau derived from destabilized microtubules can form NFTs, which share aggregative properties with Aβ in AD pathogenesis. Previous studies identified multiple pathogenic infections that perpetuate total or p-tau increases in vitro[21–25]. Other recent studies demonstrated that the active binding sites of tau possess antibacterial capabilities[26]. Similar to our argument for a physiological role of Aβ, p-tau may, likewise, not simply be an errant form of tau but also play a physiological role akin to that of an AMP.

Here we report that tau phosphorylation increases in response to HSV-1 infection and that p-tau localizes to cellular regions of HSV-1 infection. Moreover, we demonstrate that tau binds to HSV-1 and neutralizes infectivity. These data support a role for tau as an antiviral AMP and suggest a physiological role for aggregation of p-tau. The AMP activities of Aβ and p-tau leading to Aβ plaques and NFTs, together with neuroinflammation, suggest the possibility that AD neuropathology evolved as a multilayered and orchestrated host defense response to microbial infection in the brain.

Results

Tau inhibits HSV-1 infection and viral plaque formation/growth in human neuronal cell culture

To test for potential antiviral properties of tau, we first pretreated human ReNcell VM neuronal cell cultures (neuronal cultures) with p-tau followed by infection with HSV-1 and assessed the response of the infection to tau. Mature differentiated two-dimensional (2D) neuronal cultures were preincubated for 24 hours with synthetic 2N4R GSK-3β p-tau (synthetic p-tau) prior to infection with an mRFP-tagged HSV-1. We then employed confocal microscopy to assay single-cell infection counts as well as viral plaque counts and growth (Fig. 1a and Extended Data Fig. 1).

Preincubation with p-tau significantly attenuated both HSV-1 single-cell infection ($P < 0.05$) and HSV-1 plaque counts ($P < 0.01$) compared to untreated controls (Fig. 1). P-tau protection against HSV-1 infection was concentration dependent, with statistical significance achieved at 1.25 μg ml^{-1} (Fig. 1b–f). Pretreatment with p-tau also significantly reduced HSV-1 plaque counts based on the numbers of plaques per single-cell infection ($P < 0.05$; Fig. 1d). In addition to HSV-1 plaque formation, p-tau inhibited plaque growth ($P < 0.05$; Fig. 1e). Specifically, at 1.25 μg ml^{-1} p-tau, the highest quartile of viral plaque sizes was significantly smaller than untreated controls ($P < 0.01$; Fig. 1f). Non-phosphorylated tau isoforms had no effect on HSV-1 single-cell infections or plaque counts (Fig. 1g,h and Extended Data Fig. 1b–g).

Tau properties that increase aggregation promote binding to HSV-1 viral capsid proteins

HSV-1 is an enveloped virus that merges its lipid bilayer with the host cell during infection, allowing the capsid to gain entry. We next tested the intracellular interaction of tau with the HSV-1 capsid. For this purpose, we assayed different isoforms of tau for binding efficacy to isolated HSV-1 capsid using a modified binding ELISA as described in the Methods. Although human tau exists in six isoforms, we focused on the two most prominent forms in the central nervous system: 2N4R and 2N3R. 2N4R is the wild-type or full-length form of tau and aggregates efficiently at near physiological conditions. Additionally, full-length tau (441 amino acids) preserves the most phosphorylation sites. In a healthy adult brain, equal quantities of 3R and 4R tau isoforms are present. We chose 2N3R to represent our 3R isoform for comparison to 4R, thereby preserving the same N-terminal repeat number to isolate the comparison between the microtubule-binding domain repeats. These microtubule-binding domain repeats were previously identified as containing potential antimicrobial sequences[26,27].

We observed significantly increased binding affinity of p-tau with HSV-1 capsids compared to whole enveloped HSV-1 virions when normalized for available capsid binding targets using anticapsid antibodies VP21/VP22a ($P < 0.0001$; Fig. 2a and Extended Data Fig. 2). Similarly, we found increased tau capsid binding affinity over whole virion for all tested isoforms of tau once normalized for binding target availability, based on anticapsid antibody binding ($P < 0.0001$; Extended Data Fig. 2b). These findings suggest the possibility of intracellular binding of p-tau to HSV-1 capsid after entry of the virus into the cell.

Next, we tested various isoforms of tau for concentration-dependent binding to HSV-1 capsid ($P < 0.001$, Fig. 2c; $P < 0.0001$, Extended Data Fig. 3). Previous studies showed that increased binding repeats and phosphorylation enhance tau aggregation[28,29]. 2N4R p-tau, which contains the most microtubule-binding domain repeats, exhibited the highest binding efficiency to HSV-1 compared to both unphosphorylated tau isoforms tested, 2N3R ($P < 0.001$), 2N3R/2N4R 50/50 mix ($P < 0.001$) and 2N4R ($P < 0.05$) (Fig. 2c). As a control, the scrambled version of the AMP LL-37 was tested versus p-tau and failed to significantly bind viral capsid ($P < 0.05$; Extended Data Fig. 3e). We next investigated potential binding sites for tau on HSV-1 capsids. Immobilized HSV-1 capsid was pretreated with antibodies targeting the viral capsid scaffolding protein (VP21/VP22a), tegument proteins (VP16 and ICP4) or capsid proteins (ICP5 and UL25) prior to treatment with tau. Anti-VP21/VP22a and VP16 antibodies significantly decreased tau binding ($P < 0.0001$; Fig. 2d,e), whereas ICP4 antibodies had reduced inhibition ($P = 0.0056$; Extended Data Fig. 4b), and ICP5 and UL25 antibodies failed to inhibit tau binding (Extended Data Fig. 4a,c). To assess the importance of glycosylation of the target binding site, we preincubated p-tau with the monosaccharide mannose; p-tau failed to bind effectively to HSV-1, suggesting a glycoprotein binding mechanism similar to that of Aβ (Fig. 2f). Collectively, these data support antiherpetic activities of tau, in which tau preferentially targets intracellular HSV-1 by binding to the viral capsid.

Binding of intraneuronal tau to HSV-1 viral capsids stimulates tau aggregation

AMPs can form net-like structures trapping microbes and destabilizing membranes by targeting surface proteins and self-aggregation. We previously identified the ability of Aβ to bind surface glycoproteins on bacteria and viruses, subsequently stimulating the formation of amyloid fibrils[30–33]. Using synthetic 2N4R p-tau, we examined whether HSV-1 capsids are able to seed tau fibril formation. The interaction of HSV-1 capsid with synthetic tau was imaged by transmission electron microscopy (TEM) 24 hours after co-incubation. In a mixture consisting only of synthetic tau and purified HSV-1 capsids, we observed examples of both amorphous aggregated tau and fibril tau, serving to agglutinate multiple HSV-1 capsids together (Fig. 3a,b). Expanding on these results, we examined HSV-1-infected neuronal cultures by TEM analysis of ultramicrotomy slices. Tau was previously observed in the nucleus, nucleolus and pericentromeric heterochromatin[34–37].

https://doi.org/10.1038/s41593-025-02157-0

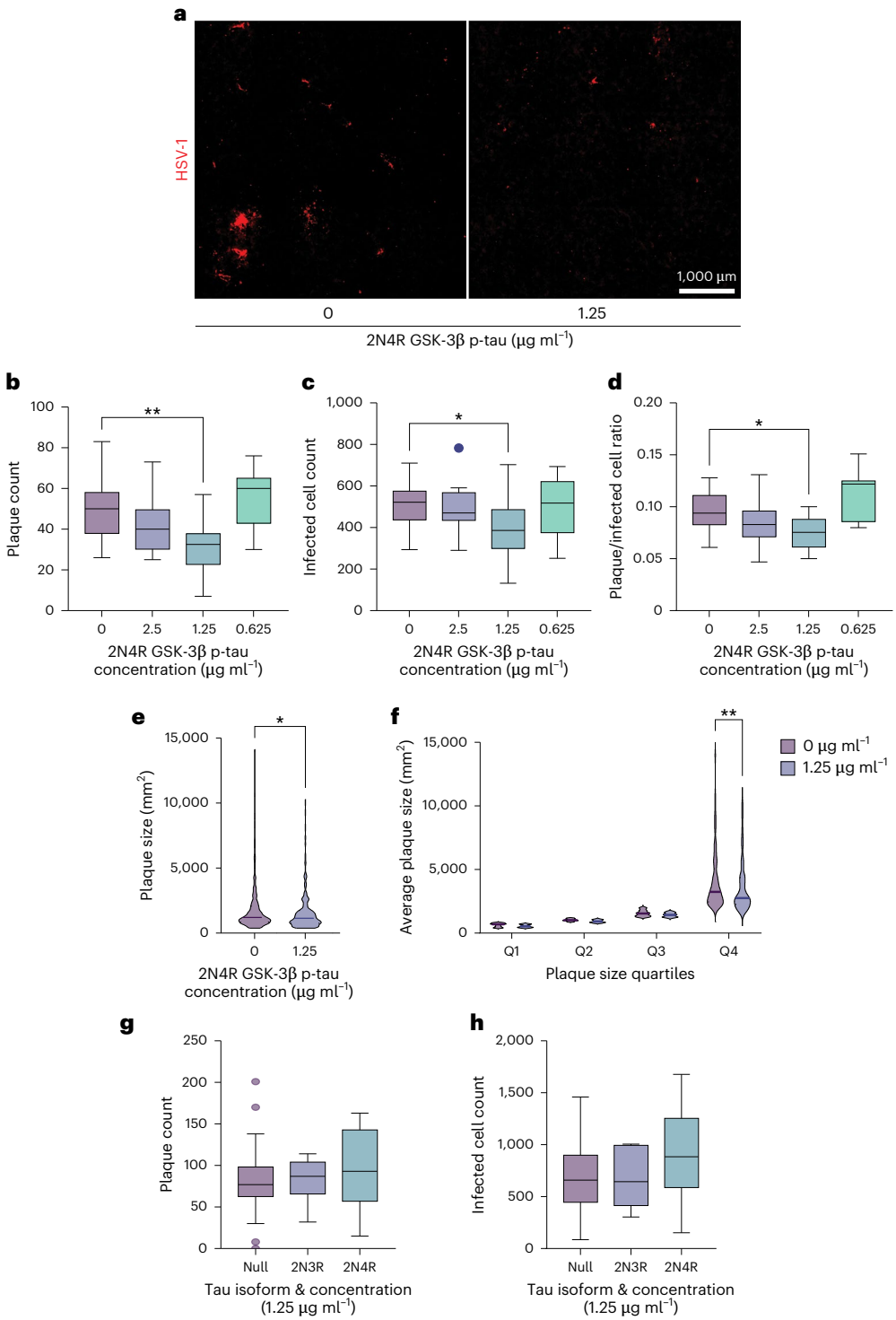

Fig. 1 | Phosphorylation of tau is key to inhibiting HSV-1 infection and viral plaque formation in 2D human neuronal cell culture. 2D ReNcell VM cultures were preincubated with dilutions of synthetic 2N3R tau, 2N4R tau or 2N4R GSK-3β p-tau followed by HSV-1 infection to assay the antimicrobial protective properties of tau. After HSV-1 infection, whole wells were imaged by confocal microscopy and analyzed for red fluorescence. **a**, Images comparing HSV-1 plaque formation in the absence or presence of 2N4R GSK-3β p-tau (1.25 µg ml^{-1}). **b**–**f**, Whole-well images from the 2N4R GSK-3β p-tau (scale of 2.5 µg ml^{-1} to 0.625 µg ml^{-1}) pretreated conditions were analyzed using Nikon Elements GA3 to compare the number of HSV-1 plaques ($F_{3,54}$ = 7.069, $^{**}P$ = 0.0015) (**b**), the number of HSV-1 single-cell infections ($F_{3,54}$ = 2.754, $^{*}P$ = 0.0291) (**c**), the ratio of plaques to single-cell infections ($F_{3,54}$ = 6.428, $^{*}P$ = 0.0169) (**d**), the size of individual HSV-1 plaques by area ($^{*}P$ = 0.0260) (**e**), and the average size of HSV-1 plaques by area distributed into quadrants ($F_{3,1,376}$ = 1.859, $^{**}P$ = 0.0022) (**f**). In addition, whole well images from the 2N3R and 2N4R tau conditions (1.25 µg ml^{-1}) were analyzed using Nikon Elements General Analysis 3 (GA3) to compare the number of HSV-1 plaques (**g**) and the number of HSV-1 single-cell infections (**h**). Box plots are representative of ±s.e.m. (n = 11) depicting median and interquartile range, with whiskers denoting variability according to Tukey's method. Statistical mean comparisons were calculated by one-way ANOVA using Dunnett's multiple comparisons test (**b**–**d**), one-way ANOVA using Tukey's multiple comparisons test (**g**,**h**), two-tailed Kolmogorov–Smirnov test (**e**) for plaque size distribution and two-way ANOVA using Sidak's multiple comparisons test (**f**).

https://doi.org/10.1038/s41593-025-02157-0

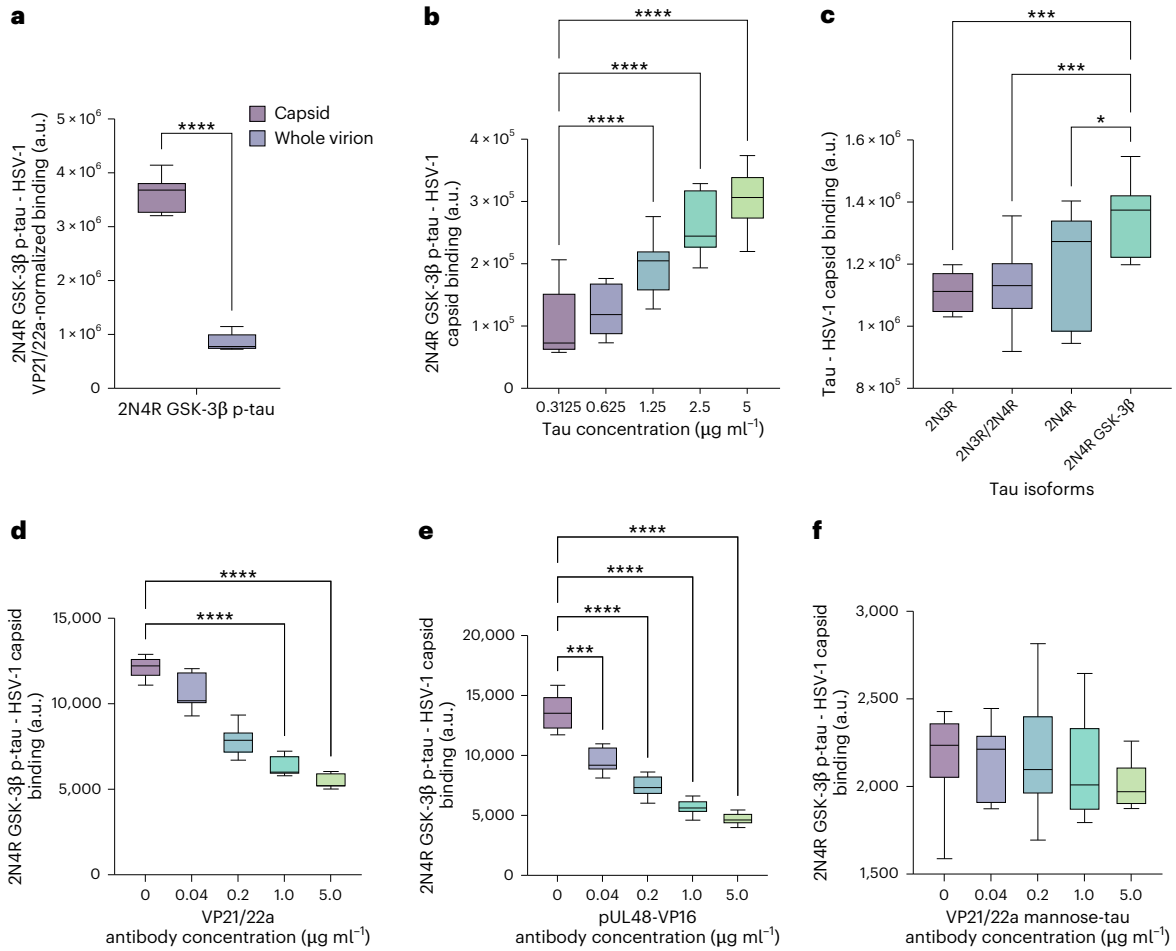

Fig. 2 | Tau binding to HSV-1 viral capsid proteins is potentiated by microtubule-binding repeats and phosphorylation. Dilutions of synthetic tau isoforms were incubated with heat-immobilized HSV-1 capsid or whole virion in indirect and competitive ELISAs to measure tau–virus binding affinity. **a**, 2N4R GSK-3β p-tau binding between HSV-1 isolated capsid or whole virion was compared after normalization of available binding sites assessed using VP21/VP22a antibody (****$P < 0.0001$). **b**, Dilutions of 2N4R GSK-3β p-tau (scale of 5 μg ml^{-1} to 0.3125 μg ml^{-1}) were incubated with immobilized HSV-1 capsids ($F_{4,55} = 43.18$, ****$P < 0.0001$). **c**, The binding affinity of 2N4R GSK-3β p-tau to HSV-1 capsids was compared to 2N3R, 50/50 mix of 2N3R/2N4R and 2N4R tau ($F_{3,44} = 8.996$, *$P = 0.267$ ((2N4R GSK-3β p-tau versus 2N3R tau, ***$P = 0.0007$), (2N4R GSK-3β p-tau versus 2N3R/2N4R tau, ***$P = 0.0007$)). **d**,**e**, Tau adhesion inhibition was assessed by preincubation of immobilized HSV-1 capsids with an anti-VP21/VP22a antibody ($F_{8,32} = 7.071$, ****$P < 0.0001$) (**d**) or an anti-pUL48-VP16 antibody ($F_{8,32} = 3.978$, ***$P = 0.004$, ****$P < 0.0001$) (**e**) before exposure to 2N4R GSK-3β p-tau. **f**, Tau adhesion inhibition was repeated with the anti-VP21/VP22a antibody using a mannose-incubated 2N4R GSK-3β p-tau. Box plots are representative of ±s.e.m. ($n = 12$) depicting median and interquartile range, with whiskers denoting variability according to Tukey's method. Statistical significance was calculated by two-tailed Mann–Whitney test (**a**) and one-way ANOVA using Tukey's multiple comparisons test (**b**–**f**).

Using the anti-p-tau antibody (PHF1) labeled with immunogold nanoparticles to identify phosphorylated tau, we observed the association of tau with the surface of HSV-1 capsids in cellular nuclei (Fig. 3c,d).

HSV-1 induces intraneuronal aggregation of p-tau and neuritic dystrophy

HSV-1 infection of murine neurons or human neuroblastoma cell cultures was previously reported to increase hyperphosphorylated tau, interpreted as an abnormal by-product of viral infection[21,22]. To examine the response of tau to HSV-1 infection in a neuronal environment, we infected 3D neuronal cultures and used PHF1 to assay for intraneuronal aggregation of p-tau in dystrophic neurites and cell bodies. We examined p-tau-stained cells 24 hours after infection using confocal microscopy. Consistent with HSV-1-driven aggregation of p-tau, we observed significant increases in p-tau-positive dystrophic neurites ($P < 0.01$) and neuronal soma ($P < 0.001$) compared to uninfected neuronal cultures (Fig. 4a–c). Co-localization of p-tau and the β-sheet staining dye, thioflavin S, confirmed the presence of aggregated p-tau during infection (Fig. 4d,e). In addition to p-tau aggregation, we observed increased anti-total tau fluorescent signal intensity and punctate distribution inside infected cells (Extended Data Fig. 5).

Next, we used ELISA using Meso Scale Discovery (MSD) to validate the aggregation of p-tau and total tau in neuronal cultures infected with HSV-1. We observed a significant dose-dependent increase in the insoluble-to-soluble p-tau ratio and total tau after HSV-1 infection ($P < 0.0001$; Fig. 4f–k). This increase in p-tau was consistent with our immunofluorescence analysis, suggesting that the aggregated p-tau observed in dystrophic neurites and cell bodies is insoluble p-tau. Variability in p-tau distribution was observed via immunofluorescence analysis between PHF1 and Thr231 (antibody used in MSD) (Extended Data Fig. 6). Compared to uninfected cells, we did not observe any cytotoxicity for cell death as assayed by lactate dehydrogenase (LDH) assay at any HSV-1 infection concentrations (Extended Data Fig. 7).

HSV-1 infection promotes release of p-tau and increased presence of p-tau in adjacent neurons

After HSV-1 infection, we observed a significant decrease in levels of intracellular soluble p-tau (−48.8%, $P < 0.0001$; Fig. 4f). In the absence

https://doi.org/10.1038/s41593-025-02157-0

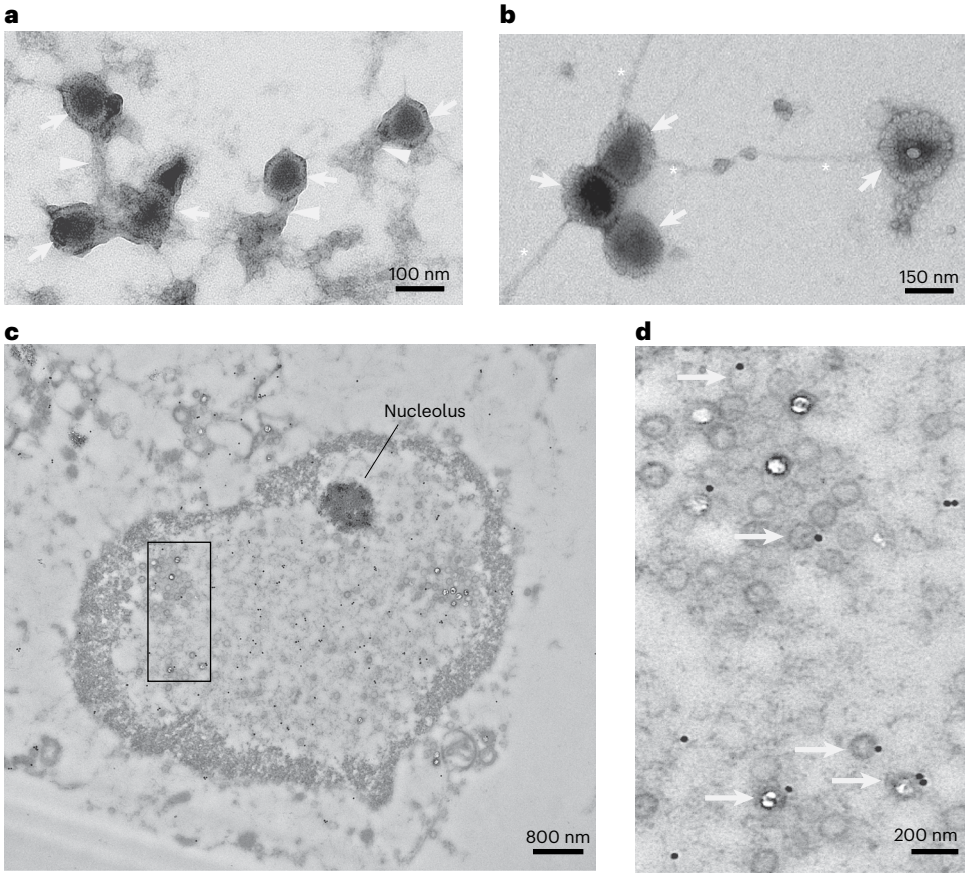

Fig. 3 | HSV-1 capsids bind to intraneuronal tau and stimulate aggregation. Co-incubated isolated HSV-1 capsids and 2N4R GSK-3β p-tau were analyzed by TEM. **a**,**b**, Co-incubated HSV-1 capsid (arrows) and 2N4R GSK-3β p-tau displayed amorphous tau aggregates (triangles) and fibrillar tau structures (*) emanating from viral capsid surfaces. **c**, 3D ReNcell VM cultures infected with HSV-1 were sliced and probed with anti-p-tau-Au nanoparticles. **d**, Inside the cell nucleus, HSV-1 capsids were identified with anti-p-tau-Au binding on their surface (arrows). Micrographs are representative of data from multiple discrete imaging fields ($n = 3$).

of significant cell death (Extended Data Fig. 7), this decrease suggested a release or expulsion of p-tau after HSV-1 infection. To examine the movement of p-tau after HSV-1 infection, we measured and compared p-tau and total tau levels between culture media and cell lysates from infected and uninfected neuronal cultures. We observed significant increases in the p-tau to total tau ratios in the media (141.8%, $P < 0.0001$) (Fig. 5a–c), whereas there was a simultaneous, significant decrease in the soluble p-tau to total tau ratio in the cell lysates (−54.6%, $P < 0.0001$) (Fig. 5d). To examine whether increased extracellular p-tau influences surrounding cells as an AMP, we assessed neuronal cultures in a microfluidic device. These devices were constructed with microchannels connecting enclosed compartments on either side. This design allowed for the isolation of the initial location of HSV-1 infection and restricted the spread through microchannels to the adjacent compartments, thereby preventing uncontrolled infection of the culture. Immunofluorescent analysis of HSV-1 (mRFP) and p-tau (anti-p-tau tagged with fluorescent secondary) revealed a significant increase in p-tau fluorescence intensity inside uninfected cells in proximity to HSV-1-infected cells when compared to uninfected cells not in proximity to the infection (26.9%, $P < 0.001$; Fig. 5e,f). We also noted a strong correlation between p-tau intensity and the viral load in proximity to the uninfected cells (Fig. 5g). Interestingly, the uninfected cells in close proximity to infection revealed no changes in total tau levels (Extended Data Fig. 5a,b). When comparing viral load to total tau intensity in uninfected cells residing proximally to infected cells, unlike p-tau, there was no correlation with total tau levels. This finding further reinforces the observed response of p-tau specific to viral infection (Extended Data Fig. 5c). These results are consistent with the notion that preincubation with p-tau provided protection from HSV-1 infection and reduced viral plaque growth (Fig. 1). These data suggest that extracellular p-tau may stimulate the generation of p-tau in adjacent cells or promote endocytosis of p-tau released into the media, thereby providing increased protection from HSV-1 infection in close proximity[38].

Internalized extracellular p-tau promotes intracellular p-tau through non-IFNγ inflammatory pathway

The increased presence of p-tau in uninfected cells proximal to infection sites (Fig. 5e–g) along with the increase of soluble p-tau into the media (Fig. 5a–d) suggest that p-tau may be involved in cell-to-cell transfer as part of its antimicrobial action. To test this mechanism, we utilized a novel two-culture system wherein we seeded a ReNcell VM culture in a well insert with a 0.1-µm filter at the bottom and incubated it with azide-labeled amino acids. Once mature, we infected the culture with HSV-1 and subsequently transferred the insert to a well with mature uninfected 3D ReNcell VM cultures. The 0.1-µm pore size inhibited mature virus from transferring between cultures but allowed azide-labeled protein transfer. In this manner, we were able to interrogate protein migration in infected cell cultures.

We observed internalization of azide-positive peptides in the uninfected cultures after the addition of the well insert, but no transfer of HSV-1 or viral infection (Fig. 6a). These azide-positive peptides were confirmed to be p-tau based on significant co-localization with the p-tau antibody PHF1 (Fig. 6a–c). Consistent with our findings of

https://doi.org/10.1038/s41593-025-02157-0

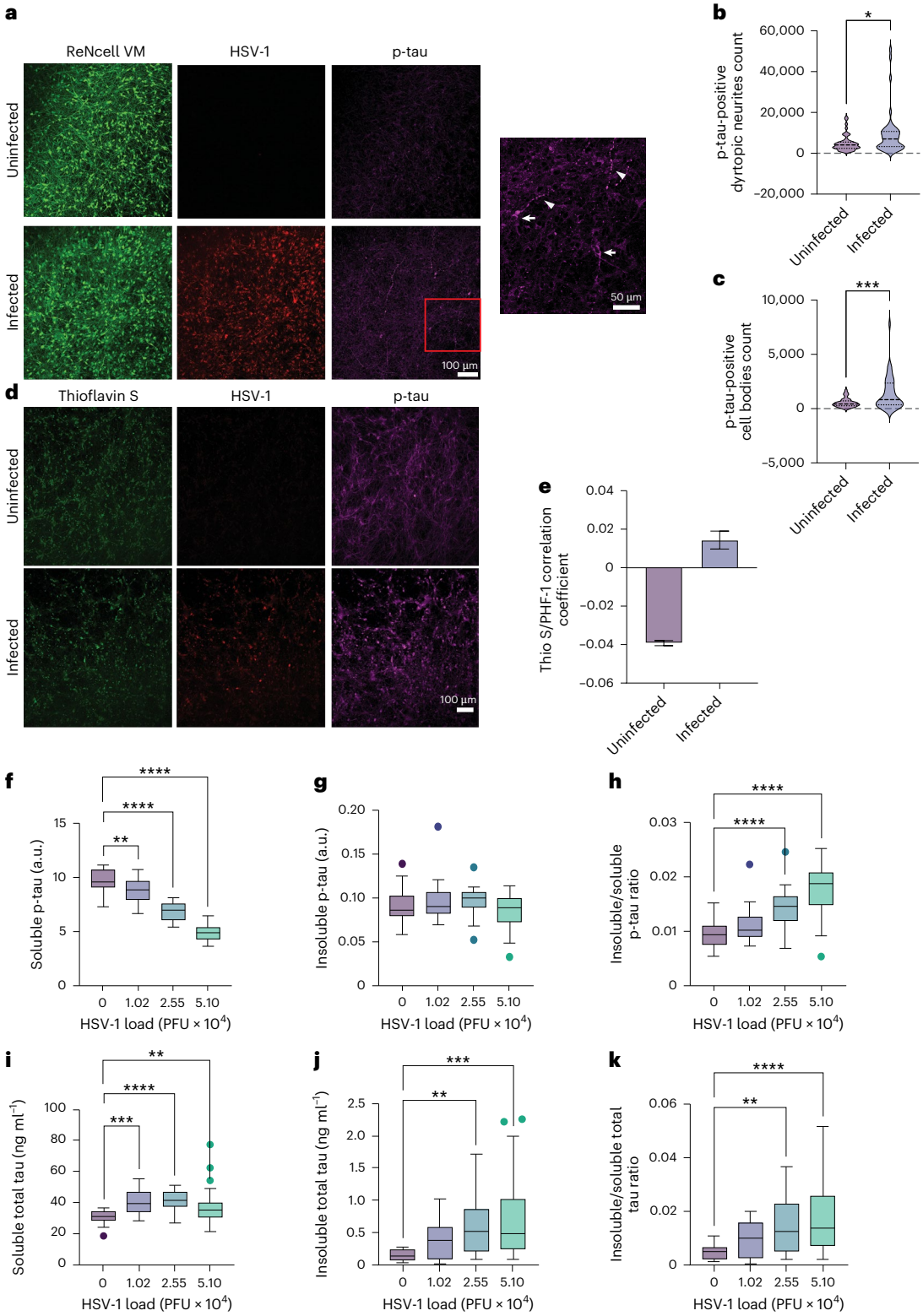

increased p-tau in uninfected cells proximal to infection (Fig. 5), we also observed a significant increase in p-tau intensity in cells that were positive for exogenous p-tau ($P < 0.0001$; Fig. 6d).

Next, we examined potential pathways responsible for promoting the increase in p-tau levels. To assess whether tau phosphorylation is necessary for the observed antimicrobial action, we infected neuronal cultures in the presence of GSK-3β kinase inhibitors. As a result, we observed a significant dose-dependent increase in viral plaque counts, cellular infections and plaque sizes with increased inhibitor (Fig. 6e and Extended Data Fig. 8). Next, we tested whether inflammation via interferon-γ (IFNγ) signaling pathway drives increases in p-tau and associated antiviral protection against HSV-1 infection versus the addition of exogenous p-tau. Under non-infectious conditions, the addition of exogenous p-tau did not elicit an inflammatory reaction as assessed by the measurement of 10 different proinflammatory cytokine levels (Fig. 6f). Similarly, attenuation of IFNγ by anti-IFNγ antibodies

Fig. 4 | HSV-1 induces intraneuronal aggregation of p-tau and neuritic dystrophy. 3D ReNcell VM cultures were infected with HSV-1 to characterize tau's change in cellular distribution and levels in response to viral infection. As shown in **a**, 3.5–4-week-old 3D ReNcell VM cultures were infected with a replication-deficient HSV-1 (deletion of UL28 protein) for 24 hours, immunoprobed with anti-p-tau (PHF1) and anti-HSV1 labeled with a fluorescent secondary antibody and analyzed for neurons (GFP), HSV-1 (568) and p-tau (647) fluorescence by confocal microscopy. **b**,**c**, Fluorescent image captures from 384 wells over four experiments were compared by GA3 software in Nikon Elements for p-tau fluorescent neurites (triangles) (***$P = 0.0002$) (**b**) and cell bodies (arrows) (*$P = 0.0022$) (**c**) between uninfected and infected wells. **d**, Confocal images showing 3D ReNcell VM cultures that were infected with HSV-1 for 24 hours, immunoprobed with anti-p-tau (PHF1) labeled with a fluorescent secondary antibody and immunostained with thioflavin S. **e**, Pearson's correlation coefficient (error bars represent 95% confidence interval) was derived from analyzing uninfected and infected wells for co-localization of thioflavin S (green), HSV-1 (RFP) and p-tau (647) fluorescence. **f**–**k**, 3.5–4-week-old 3D ReNcell VM cultures were infected with serial dilutions of HSV-1 for 24 hours, and cell lysates were separated into soluble and insoluble tau fractions for analysis by MSD Multi-Spot Phospho (Thr 231)/Total Tau Assay. **f**, Comparison of cellular soluble p-tau at different viral loads ($F_{3,96} = 129.6$, **$P = 0.0027$, ****$P < 0.0001$). **g**, Comparison of cellular insoluble p-tau at different viral loads. **h**, Comparison of the ratio between cellular insoluble and soluble p-tau at different viral loads ($F_{3,96} = 26.54$, ****$P < 0.0001$). **i**, Comparison of cellular soluble total tau at different viral loads ($F_{3,96} = 9.251$, **$P = 0.0040$, ***$P = 0.0001$, ****$P < 0.0001$). **j**, Comparison of cellular insoluble total tau at different viral loads ($F_{3,89} = 6.810$, **$P = 0.0049$, ***$P = 0.0002$). **k**, Comparison of the ratio between cellular insoluble and soluble total tau at different viral loads ($F_{3,89} = 7.469$, **$P = 0.0057$, ****$P < 0.0001$). Box plots are representative of ±s.e.m. ((**f**–**h**, $n = 25$), (**i**–**k**, $n = 19$)) depicting median and interquartile range, with whiskers denoting variability according to Tukey's method. Statistical mean comparisons were calculated by two-tailed unpaired *t*-tests (**b**,**c**) and one-way ANOVA using Dunnett's multiple comparisons test (**f**–**k**).

after HSV-1 infection did not exacerbate HSV-1 infection (Fig. 6g,h and Extended Data Fig. 9). Interestingly, anti-IFNγ antibody treatment neutralized the protective effects of synthetic p-tau pretreatment, indicating that an IFNγ-mediated pathway is important for the anti-microbial action of p-tau (Fig. 6g). In conjunction with our findings of p-tau aggregation and spread in the presence of infection (Figs. 4 and 5), these data provide compelling evidence for the antiviral activity of p-tau by both protecting against and modulating an innate immune response to HSV-1.

Both HSV-1 and p-tau aggregates are phagocytosed by microglia in a 3D neural–glial triculture model of AD

Microglia are essential to the central nervous system (CNS) response to HSV-1 infection by identifying viral pathogen-associated molecular patterns (PAMPs), releasing inflammatory cytokines and clearing virus and damaged neurons. Interestingly, microglia were recently suggested to contribute to pathogenic tau spread due to endocytosis of tau aggregates and subsequent failure to fully digest the aggregates, followed by secretion of exosomes containing 'tau seeds'[39]. To investigate the interaction among tau, HSV-1 and microglia, we seeded a neuronal/astrocytic 3D ReNcell VM culture with microglia derived from induced pluripotent stem cells and then infected the neural–glial tricultures with HSV-1. Twenty-four hours after infection, the cultures were fixed and prepared for immunocytochemistry (ICC) with anti-IBA1 and anti-p-tau (PHF1) antibodies. Co-localization of p-tau and HSV-1 was observed inside IBA1-positive microglial cells, which was not present in uninfected controls (Fig. 7). Although more experimentation is necessary to determine whether the p-tau/HSV-1 is being phagocytosed as an independent complex or as part of infected neurons, these results warrant more detailed studies addressing microglia internalizing p-tau/HSV-1 complexes.

Discussion

Evidence for a microbial component to the etiology and pathogenesis of AD has continued to grow over the last decade. Although a consensus on particular pathogens has still not been reached, animal studies, retrospective cohort studies for infection and AD risk and microbiome screens have all identified the epidemiological prevalence of microbes in dementia and pathogen-driven shifts in locations such as the gut microbiota that may promote AD-related neuropathology[40–43]. Furthermore, these studies are supported by multiple comprehensive studies of particular microbes[44–48]. Previously, we reported antimicrobial properties of Aβ based on its ability to neutralize *Salmonella*, HSV-1 and human herpesvirus 6 (HHV-6) (refs. 10,11). These studies led to the Antimicrobial Protection Hypothesis of AD, postulating that Aβ has evolved to protect the brain against infection, with amyloid plaques serving as extracellular traps for microbes. As a corollary to this idea, the gene mutations that predispose to AD pathology, today, may have been conserved in evolution owing to their ability to enhance innate immunity in the brain[14].

In the present study, we reveal a notable novel role for tau as an antiviral protein against HSV-1, based on affording increased protection from infection (Fig. 1) and highly effective binding to HSV-1 to neutralize the virus (Figs. 2 and 3). We also observed an infection-based response with the phosphorylation of tau and the resulting p-tau shifting to an insoluble form (Fig. 4) and increased p-tau presence in uninfected cells in proximity to the location of infection (Fig. 5). The sequestration of p-tau into insoluble forms enhances innate immunity by binding HSV-1 (Fig. 3), destabilizing microtubules, breaking down fast axonal transport and generating NFTs, all of which would serve to hamper neurotropic spread of virus across synapses from one neuron to another. These findings are consistent with the oligomerization of AMPs as an essential characteristic for their innate immune functions[49,50].

Fig. 5 | HSV-1 promotes the release of p-tau from infected neurons and the accumulation of p-tau in uninfected neurons adjacent to infection. ReNcell VM cultures were infected with HSV-1 for 24 hours to characterize p-tau's extracellular release and changes in proximity to viral infection. **a**–**d**, 3.5–4-week-old 3D ReNcell VM cultures were infected with serial dilutions of HSV-1 for 24 hours, and cell media and cell lysates were analyzed by MSD Multi-Spot Phospho (Thr 231)/Total Tau Assay for soluble p-tau and total tau. **a**, Comparison of cell media soluble p-tau at different viral loads ($F_{3,54} = 7.521$ ((uninfected versus 2.55, ***$P = 0.0005$), (uninfected versus 5.10, ***$P = 0.0004$)). **b**, Comparison of cell media soluble total tau at different viral loads ($F_{3,55} = 10.49$, **$P = 0.0011$). **c**, Comparison of the ratio between cell media p-tau and total tau at different viral loads ($F_{3,54} = 19.94$, ****$P < 0.0001$). **d**, Comparison of the ratio between cell lysate soluble p-tau and soluble total tau at different viral loads ($F_{3,96} = 202.5$, ****$P < 0.0001$). **e**, 2D ReNcell VM cultures in microfluidic devices were infected in the left chamber with HSV-1 for 48 hours, immunoprobed with anti-p-tau (PHF1) labeled with a fluorescent secondary antibody and analyzed for neurons (GFP), HSV-1 (RFP) and p-tau (647) fluorescence by confocal microscopy. Fluorescence signals for ReNcell VM, HSV-1 and p-tau were imaged for infected and uninfected conditions. **f**, GA3 analysis of HSV-1-positive neurons compared intracellular p-tau fluorescence among infected neurons (triangles), uninfected neurons proximal to infected neurons (*) and uninfected neurons not proximal to infected neurons (arrows) ($F_{2,3,288} = 45.35$, ****$P < 0.0001$). **g**, Individual neuronal p-tau fluorescence intensity was compared to total proximal HSV-1–RFP fluorescence intensity ($R^2 = 0.7912$). Box plots are representative of ±s.e.m. ((**a**–**c**, $n = 13$), (**d**, $n = 25$)) depicting median and interquartile range, with whiskers denoting variability according to Tukey's method. Statistical mean comparisons were calculated by one-way ANOVA using Dunnett's multiple comparisons test (**a**–**d**), one-way ANOVA using Tukey's multiple comparisons test (**f**) and simple linear regression (**g**).

https://doi.org/10.1038/s41593-025-02157-0

Previous research on antimicrobial properties of tau by Kobayashi et al.[26] reported that tau peptide fragments of the microtubule-binding site possessed strong antimicrobial activities against *Staphylococcus aureus* and *Escherichia coli*. Although it was hypothesized that this binding activity was driven by negatively charged surfaces of Gram-negative bacteria, we observed preferential binding to viral capsid over viral envelope (Fig. 2a and Extended Data Fig. 2b), despite the strong negative charge of the envelope from post-translational additions of sialic acid to the glycoproteins on the envelope surface, suggesting a more specific targeting beyond peptide charge[51]. A subsequent study by Powell-Doherty et al.[52] examined Aβ and p-tau as components of an anti-threat response to HSV-1, demonstrating viral-induced phosphorylation of tau and accumulation of Aβ oligomers. They propose that p-tau does not inhibit viral replication and may alternatively be a danger-associated molecular pattern (DAMP). By contrast, our data support the direct role of p-tau in viral inhibition and binding (Figs. 1–3).

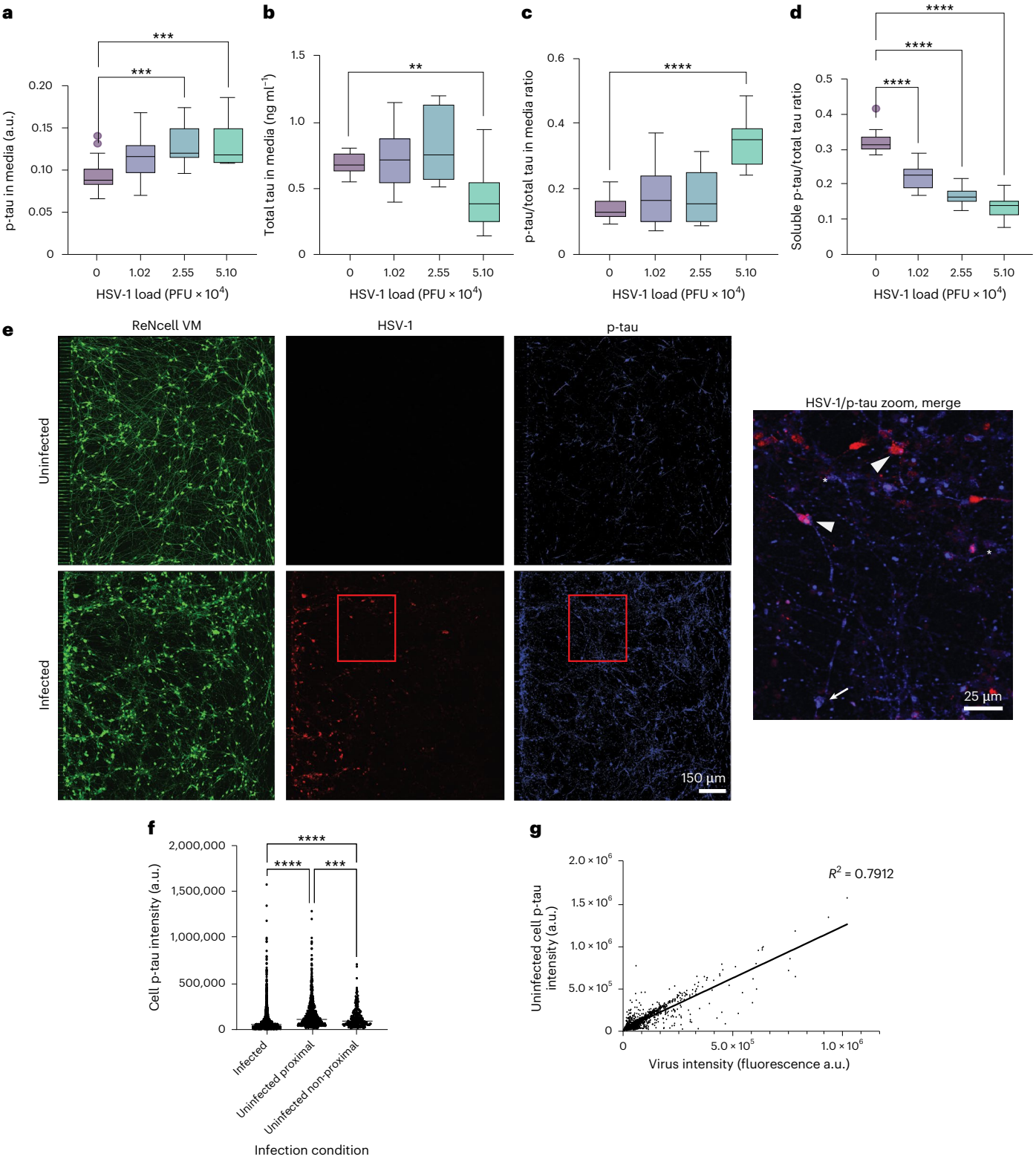

https://doi.org/10.1038/s41593-025-02157-0

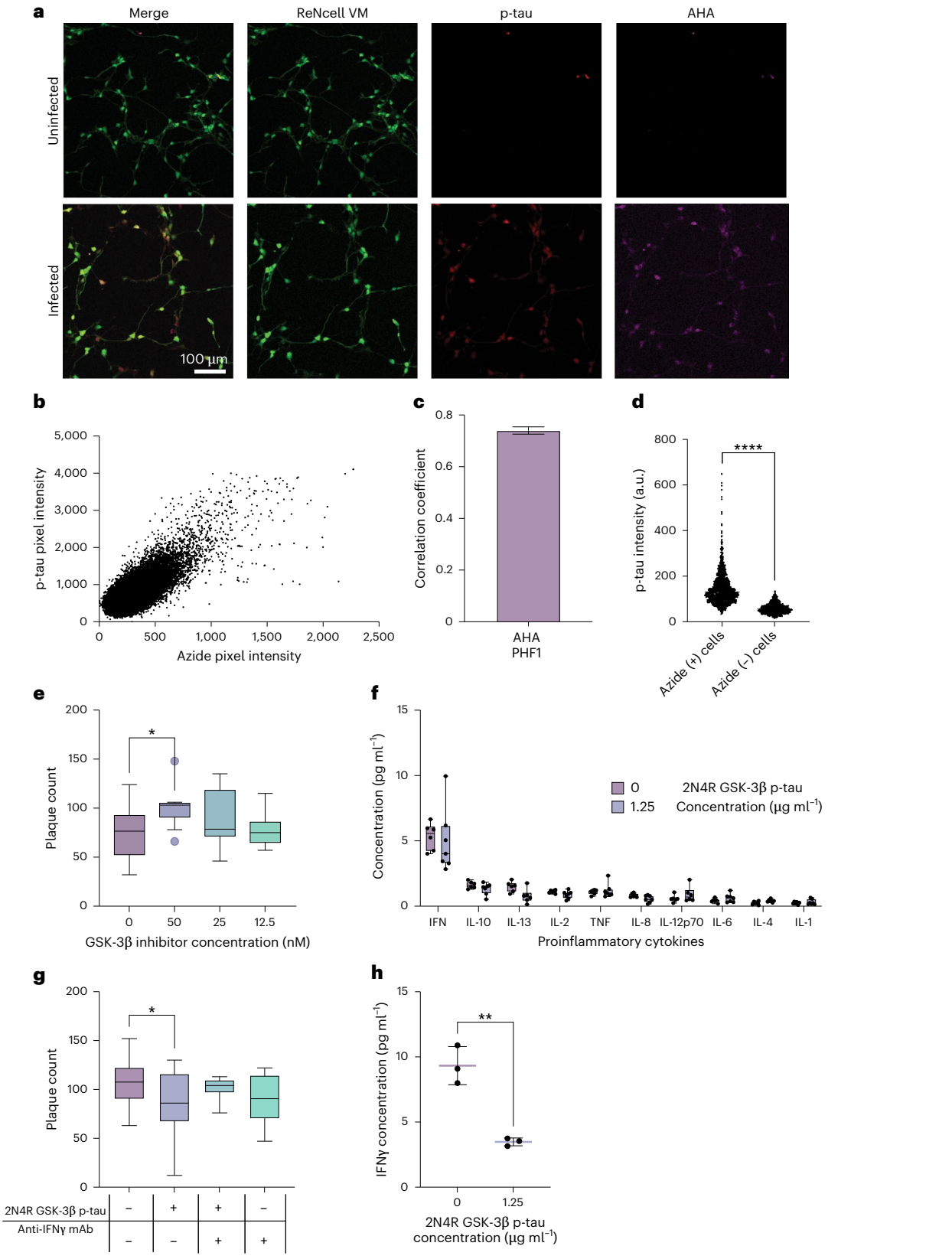

Utilizing antibodies against different viral and capsid peptides for steric interference of p-tau binding, we observed targeted binding of p-tau to a region occupied by inner tegument proteins. Blocking major capsid protein ICP5 or capsid stabilizing protein UL25 failed to inhibit p-tau binding entirely (Extended Data Fig. 4a,c), whereas blocking tegument-associated protein ICP4 led to modest inhibition (Extended Data Fig. 4b). Conversely, antibodies against tegument proteins VP21/22a and VP16 led to significant dose-dependent inhibition of p-tau binding to viral capsid (Fig. 2d,e). Notably, inner tegument protein VP1/VP2 binds VP16, VP16 binds VP22 and all three of these viral proteins are essential for the bidirectional transport of HSV-1 capsids along microtubules[53,54]. These data suggest a dual-action

Fig. 6 | Exogenous p-tau induces phosphorylation for essential antiviral activity. ReNcell VM cultures were infected with HSV-1 to determine the degree of immune response. **a**, One-week-old 2D ReNcell VM uninfected and infected cultures were immunoprobed with L-azidohomoalanine (AHA) and anti-p-tau (PHF1) and then labeled with fluorescent secondary antibodies and analyzed for neurons (GFP), p-tau (594) and AHA (647) fluorescence by confocal microscopy. **b**, Distribution plot of individual AHA and p-tau pixel intensities after infection. **c**, Pearson's correlation coefficient (error bars represent 95% confidence interval) of images of internalized AHA and PHF1 in ReNcell VM cells. **d**, Fluorescent image captures from nine wells over three experiments were compared by GA3 software in Nikon Elements for p-tau fluorescence (****$P < 0.0001$) between azide-positive and azide-negative cells. **e**, One-week-old 2D ReNcell VM cultures were preincubated with dilutions of a GSK-3β inhibitor (scale of 50 nM to 25 nM) for 24 hours followed by a 24-hour HSV-1 infection and imaged by confocal microscopy for red fluorescence. Whole-well images were analyzed using Nikon Elements GA3 to compare the number of HSV-1 plaques between conditions ($F_{3,53} = 2.806$, *$P = 0.0268$). **f**,**h**, Conditioned media collected from 1-week-old ReNcell VM uninfected (**f**) and 1-hour HSV-1 infected (**h**) ($F_{2,2} = 23.85$, **$P = 0.0025$) cultures pretreated with 2N4R GSK-3β p-tau (1.25 μg ml^{-1}) were run on a proinflammatory cytokine MSD. **g**, One-week-old 2D ReNcell VM cultures were preincubated with 2N4R GSK-3β p-tau (1.25 μg ml^{-1}) and anti-IFNγ antibody (10 μg ml^{-1}) for 24 hours followed by a 24-hour HSV-1 infection and imaged by confocal microscopy for red fluorescence. Whole-well images were analyzed using Nikon Elements GA3 to compare the number of HSV-1 plaques between conditions ($F_{3,56} = 4.863$, *$P = 0.0386$). Box plots are representative of ±s.e.m. ((**e**, $n = 11$), (**f**, $n = 6$), (**g**, $n = 15$), (**h**, $n = 3$)) depicting median and interquartile range, with whiskers denoting variability according to Tukey's method. Statistical mean comparisons were calculated by two-tailed unpaired Welch's *t*-test (**d**), one-way ANOVA using Dunnett's multiple comparisons test (**e**), two-way ANOVA using Tukey's multiple comparisons test (**f**), one-way ANOVA using Tukey's multiple comparisons test (**g**) and two-tailed unpaired *t*-test (**h**).

antiviral effect in which hyperphosphorylation dissociates tau from microtubules, destabilizing them and interrupting viral capsid transportation, and p-tau simultaneously binds to capsid/tegument proteins essential for viral microtubule transport. Although our data supporting antimicrobial properties of tau and p-tau are novel, evidence of tau modifications in response to infections was previously reported. HSV-1 infection results in hyperphosphorylation of tau in both human and mouse models[21,22,40,55,56]. In adult hippocampal neurons, p-tau levels increased after active and latent HSV-1 infection. Additionally, gingipains, exotoxins from *Porphyromonas gingivalis*, were reported to cleave tau, and the resulting fragments displayed antimicrobial properties[27].

Microtubules are essential for fast axonal transport in neurons but are also utilized by intracellular pathogens. Both viruses and bacteria utilize microtubule networks, and stabilization of the microtubules results in increased infection[57,58]. The protective effect of tau against HSV-1 infection (Fig. 1) and the increased ratio of insoluble versus soluble p-tau during infection (Fig. 4h,k) suggest that destabilization of microtubules by p-tau protects against microbial utilization of the cytoskeleton to spread. This is further supported by neuritic dystrophy observed where HSV-1 was isolated with p-tau (Extended Data Fig. 10a) and p-tau aggregation in neuronal somas around HSV-1 replication in the nucleus (Extended Data Fig. 10b), in effect preventing HSV-1 access to microtubule transport required for propagation.

We also observed increased viral binding with both increased R domain repeats and phosphorylation of tau, with the synthetic 2N4R p-tau being the most effective (Fig. 2). Once again, these findings suggest that the phosphorylation and increased aggregation of tau, classically observed as a pathological feature, can be alternatively viewed as a functional feature of tau designed to bind and neutralize microbial targets more effectively. Indeed, our data support the notion that the phosphorylation of tau is not just sufficient but necessary for antimicrobial activity. Non-phosphorylated tau isoforms failed to elicit any protection against HSV-1 infection (Fig. 1), and the presence of GSK-3β inhibitor during viral infection significantly increased the viral spread (Fig. 6).

Beyond AMPs, the innate immune system utilizes cytokines for essential communication and regulation of the immune response. One such key cytokine in response to HSV-1 is IFNγ, capable of inhibiting replication, impeding viral release and disrupting microtubule organization[59–61]. To differentiate the viral-driven p-tau antimicrobial response from a generalized viral immune response, we examined the role of cytokines in our model. Utilizing an anti-INFγ antibody to block the HSV-1-induced cytokine response, we observed that the removal of IFNγ during p-tau treatment negated the p-tau antiviral protection (Fig. 6g). By contrast, anti-IFNγ antibody treatment without the addition of p-tau had no effect on viral spread (Fig. 6g). MSD analysis of cytokines revealed that exogenous p-tau did not elicit any immune response (Fig. 6f), and the presence of synthetic p-tau lowered IFNγ levels released into the media (Fig. 6h). Collectively, these data suggest that IFNγ is critical for the antiviral activity of p-tau but not via inflammatory pathways. Future studies should consider the potential relationship between the induction of tight junction protein endocytosis by IFNγ combined with the effects of IFNγ on the antiviral properties of p-tau[62].

Cell-to-cell transfer and propagation of p-tau is yet another property considered to be pathological. However, our findings suggest that this p-tau propagation may also be considered a physiological antimicrobial feature of tau. The departure of tau from the somatic space is well documented, with evidence of its traversal from cell to cell via excretion and exosomes and through synaptic clefts[63–67]. The discovery that 'pathogenic' forms of tau can self-propagate and promote the aggregation of soluble tau led to the suggestion that seeding and propagation of neuropathological tau resembles prion diseases[68]. Interestingly, a recent publication by Liu et al.[69] demonstrated that active human endogenous retrovirus infections accelerated the cell-to-cell spread of tau aggregates. Our data revealing elevated p-tau in uninfected neurons in close proximity to infected cells support and may, therefore, help explain this finding (Fig. 5). Additionally, we show that the ability of tau to protect against viral infection is enhanced by co-incubation of p-tau with neurons prior to HSV-1 infection (Fig. 1). During HSV-1 infection, we also observed a significant increase in soluble p-tau being released into the extracellular space (Fig. 5). These data suggest that 'pathological' spreading of tau may actually have evolved as an antimicrobial feature, allowing tau to protect adjacent cells prior to the establishment of a spreading viral infection.

Microglia, the resident macrophage-like cells in the brain, are an essential component of brain health, playing roles in both development and protection against trauma and pathogenic invasion. Microglia can phagocytose extracellular pathogens such as HSV-1 and bacteria that make it past the blood–brain barrier as well as damaged or necrotic cells[70,71]. The ability of microglia to take up Aβ and tau, in addition to their release of proinflammatory cytokines and chemokines, have made them a prime therapeutic target in AD. We observed co-localization of p-tau and HSV-1 inside of microglia in viral-infected 3D human neuronal/astrocytic cultures co-incubated with microglia (neural–glial tricultures), suggesting that tau may also play a role in promoting microglial uptake of HSV-1 (Fig. 7).

It is important to acknowledge that tau does not fully comply with the attributes of typical AMPs, which are typically cationic, are below 100 amino acids, display broad extracellular antimicrobial efficacy, and often harbor α-helical or β-sheet secondary structures. Although most known AMPs fall within these guidelines, there are exceptions. Although more than four times the typical size of AMP, tau shares many of these commonalities, such as cationic charge and assembly into β-sheets. Other established AMPs share some of these atypical AMP-like

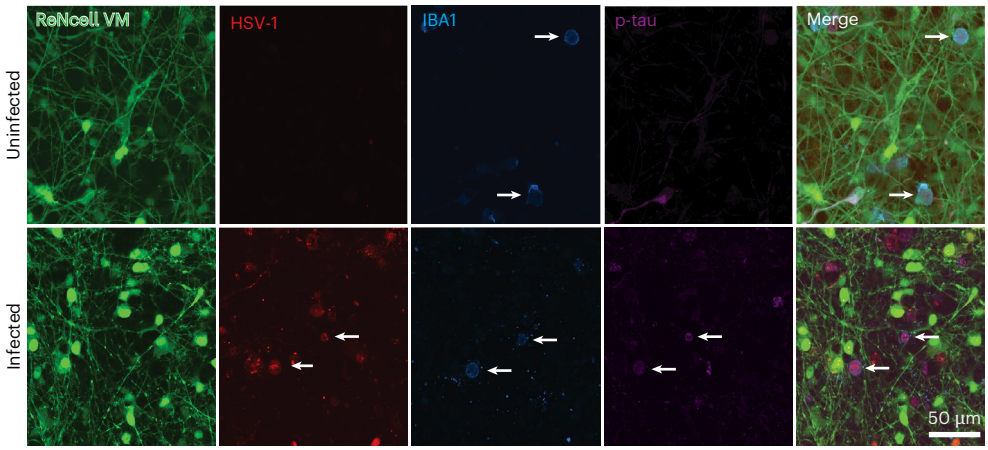

Fig. 7 | p-tau and HSV-1 co-localize inside microglia. Mature microglia were added to 3D ReNcell VM cultures prior to infection with HSV-1 to analyze the interaction among p-tau, HSV-1 and microglia. Uninfected and infected microglia–ReNcell VM cultures were immunoprobed with anti-p-tau (PHF1) and anti-IBA1 labeled with fluorescent secondary antibodies and analyzed for microglia (405), neurons (GFP), HSV-1 (RFP) and p-tau (647) fluorescence by confocal microscopy. Co-localization of HSV-1 (red) and p-tau (purple) inside of microglia (blue) was observed (arrows). Panels are representative of multiple image fields ($n = 5$).

characteristics of tau. LL-37 was found to interact with glyceraldehyde 3-phosphate dehydrogenase to immunomodulate macrophage activity[72], demonstrating an AMP capable of acting intracellularly on a host cell for immunomodulation. NONO is a nuclear protein that binds to and detects HIV capsid in the nucleus to promote cGAS-mediated innate immune activation and is 471 amino acids long[73]. Combined with our data, these unique exceptions support the notion that, although tau may not be a prototypical AMP, its physical characteristics and antimicrobial properties warrant further research into its classification as an AMP.

The data presented here strongly suggest that tau serves as a second layer of defense against pathogens in the brain. Although Aβ serves as an extracellular AMP to trap viruses in Aβ deposits, the viruses that escape and infect neurons can then be stopped by p-tau and NFTs, induced by either the virus itself or by Aβ oligomers[10]. In this manner, Aβ and p-tau combine to provide what can be considered a dual AMP host defense mechanism against viral infection. Like Aβ, tau also presents as a highly phylogenetically conserved protein, sharing the microtubule-binding domain with mammals, reptiles, birds and fish[74,75]. Our findings continue to reinforce the notion that the three major hallmarks of AD pathology—Aβ, NFTs and neuroinflammation—evolved as a multilayered and highly orchestrated host defense system as part of the innate immune system of the brain.

Online content

Any methods, additional references, Nature Portfolio reporting summaries, source data, extended data, supplementary information, acknowledgements, peer review information; details of author contributions and competing interests; and statements of data and code availability are available at https://doi.org/10.1038/s41593-025-02157-0.

References

1. Bertram, L. & Tanzi, R. E. The genetic epidemiology of neurodegenerative disease. *J. Clin. Invest.* **115**, 1449–1457 (2005).
2. Drubin, D. G. & Kirshner, M. W. Tau protein function in living cells. *J. Cell Biol.* **103**, 2739–2746 (1986).
3. Goedert, M., Spillantini, M. G., Jakes, R., Rutherford, D. & Crowther, R. A. Multiple isoforms of human microtubule-associated protein tau: sequences and localization in neurofibrillary tangles of Alzheimer's disease. *Neuron* **3**, 519–526 (1989).
4. Sexton, C. et al. Current directions in tau research: highlights from Tau 2020. *Alzheimers Dement.* **18**, 988–1007 (2022).
5. Kumar, N., Sood, D., Tomar, R. & Chandra, R. Antimicrobial peptide designing and optimization employing large-scale flexibility analysis of protein-peptide fragments. *ACS Omega* **4**, 21370–21380 (2019).
6. Ba, Z. et al. Phosphorylation as an effective tool to improve stability and reduce toxicity of antimicrobial peptides. *J. Med. Chem.* **67**, 18807–18827 (2024).
7. Chen, P. et al. Aggregation-prone antimicrobial peptides target gram-negative bacterial nucleic acids and protein synthesis. *Acta Biomater.* **192**, 446–460 (2025).
8. Diamond, G., Beckloff, N., Weinberg, A. & Kisich, K. O. The roles of antimicrobial peptides in innate host defense. *Curr. Pharm. Des.* **15**, 2377–2392 (2009).
9. Territo, M. C., Ganz, T., Selsted, M. E. & Lehrer, R. Monocyte-chemotactic activity of defensins from human neutrophils. *J. Clin. Invest.* **84**, 2017–2020 (1989).
10. Eimer, W. A. et al. Alzheimer's disease-associated β-amyloid is rapidly seeded by herpesviridae to protect against brain infection. *Neuron* **99**, 56–63 (2018).
11. Kumar, D. K. V. et al. Amyloid-β peptide protects against microbial infection in mouse and worm models of Alzheimer's disease. *Sci. Transl. Med.* **8**, 340ra72 (2016).
12. White, M. R. et al. Alzheimer's associated β-amyloid protein inhibits influenza A virus and modulates viral interactions with phagocytes. *PLoS ONE* **9**, e101364 (2014).
13. Bourgade, K. et al. β-Amyloid peptides display protective activity against the human Alzheimer's disease-associated herpes simplex virus-1. *Biogerontology* **16**, 85–98 (2015).
14. Moir, R. D., Lathe, R. & Tanzi, R. E. The antimicrobial protection hypothesis of Alzheimer's disease. *Alzheimers Dement.* **14**, 1602–1614 (2018).
15. Choi, S. H. et al. A three-dimensional human neural cell culture model of Alzheimer's disease. *Nature* **515**, 274–278 (2014).
16. Zhang, Y. et al. Amyloid-β toxicity modulates tau phosphorylation through the PAX6 signalling pathway. *Brain J. Neurol.* **144**, 2759–2770 (2021).
17. Busciglio, J., Lorenzo, A., Yeh, J. & Yankner, B. A. β-Amyloid fibrils induce tau phosphorylation and loss of microtubule binding. *Neuron* **14**, 879–888 (1995).
18. Kwak, S. S. et al. Amyloid-β42/40 ratio drives tau pathology in 3D human neural cell culture models of Alzheimer's disease. *Nat. Commun.* **11**, 1377 (2020).

19. Smith, G. A., Pomeranz, L., Gross, S. P. & Enquist, L. W. Local modulation of plus-end transport targets herpesvirus entry and egress in sensory axons. *Proc. Natl Acad. Sci. USA* **101**, 16034–16039 (2004).
20. Lindwall, G. & Cole, R. D. Phosphorylation affects the ability of tau protein to promote microtubule assembly. *J. Biol. Chem.* **259**, 5301–5305 (1984).
21. Alvarez, G., Aldudo, J., Alonso, M., Santana, S. & Valdivieso, F. Herpes simplex virus type 1 induces nuclear accumulation of hyperphosphorylated tau in neuronal cells. *J. Neurosci. Res.* **90**, 1020–1029 (2012).
22. Wozniak, M. A., Frost, A. L. & Itzhaki, R. F. Alzheimer's disease-specific tau phosphorylation is induced by herpes simplex virus type 1. *J. Alzheimers Dis.* **16**, 341–350 (2009).
23. Torres, L. et al. *Toxoplasma gondii* alters NMDAR signaling and induces signs of Alzheimer's disease in wild-type, C57BL/6 mice. *J. Neuroinflammation* **15**, 57 (2018).
24. Wang, X.-L. et al. *Helicobacter pylori* filtrate induces Alzheimer-like tau hyperphosphorylation by activating glycogen synthase kinase-3β. *J. Alzheimers Dis.* **43**, 153–165 (2015).
25. Dominy, S. S. et al. *Porphyromonas gingivalis* in Alzheimer's disease brains: evidence for disease causation and treatment with small-molecule inhibitors. *Sci. Adv.* **5**, eaau3333 (2019).
26. Kobayashi, N., Masuda, J., Kudoh, J., Shimizu, N. & Yoshida, T. Binding sites on tau proteins as components for antimicrobial peptides. *Biocontrol Sci.* **13**, 49–56 (2008).
27. Kanagasingam, S., von Ruhland, C., Welbury, R. & Singhrao, S. K. Antimicrobial, polarizing light, and paired helical filament properties of fragmented tau peptides of selected putative gingipains. *J. Alzheimers Dis.* **89**, 1279–1291 (2022).
28. Chang, E., Kim, S., Schafer, K. N. & Kuret, J. Pseudophosphorylation of tau protein directly modulates its aggregation kinetics. *Biochim. Biophys. Acta* **1814**, 388–395 (2011).
29. Zhong, Q., Congdon, E. E., Nagaraja, H. N. & Kuret, J. Tau isoform composition influences rate and extent of filament formation. *J. Biol. Chem.* **287**, 20711–20719 (2012).
30. Galzitskaya, O. V. et al. Amyloidogenic peptides: new class of antimicrobial peptides with the novel mechanism of activity. *Int. J. Mol. Sci.* **23**, 5463 (2022).
31. Torrent, M., Pulido, D., Nogués, M. V. & Boix, E. Exploring new biological functions of amyloids: bacteria cell agglutination mediated by host protein aggregation. *PLoS Pathog.* **8**, e1003005 (2012).
32. Bednarska, N. G. et al. Protein aggregation as an antibiotic design strategy. *Mol. Microbiol.* **99**, 849–865 (2016).
33. Ezzat, K. et al. The viral protein corona directs viral pathogenesis and amyloid aggregation. *Nat. Commun.* **10**, 2331 (2019).
34. Loomis, P. A., Howard, T. H., Castleberry, R. P. & Binder, L. I. Identification of nuclear tau isoforms in human neuroblastoma cells. *Proc. Natl Acad. Sci. USA* **87**, 8422–8426 (1990).
35. Rady, R. M., Zinkowski, R. P. & Binder, L. I. Presence of tau in isolated nuclei from human brain. *Neurobiol. Aging* **16**, 479–486 (1995).
36. Diez, L. & Wegmann, S. Nuclear transport deficits in tau-related neurodegenerative diseases. *Front. Neurol.* **11**, 1056 (2020).
37. Mansuroglu, Z. et al. Loss of Tau protein affects the structure, transcription and repair of neuronal pericentromeric heterochromatin. *Sci. Rep.* **6**, 33047 (2016).
38. Li, A. et al. IFN-γ promotes τ phosphorylation without affecting mature tangles. *FASEB J.* **29**, 4384–4398 (2015).
39. Brelstaff, J. H. et al. Microglia become hypofunctional and release metalloproteases and tau seeds when phagocytosing live neurons with P301S tau aggregates. *Sci. Adv.* **7**, eabg4980 (2021).
40. De Chiara, G. et al. Recurrent herpes simplex virus-1 infection induces hallmarks of neurodegeneration and cognitive deficits in mice. *PLoS Pathog.* **15**, e1007617 (2019).
41. Sipilä, P. N. et al. Hospital-treated infectious diseases and the risk of dementia: a large, multicohort, observational study with a replication cohort. *Lancet Infect. Dis.* **21**, 1557–1567 (2021).
42. Sun, J. et al. Hospital-treated infections in early- and mid-life and risk of Alzheimer's disease, Parkinson's disease, and amyotrophic lateral sclerosis: a nationwide nested case-control study in Sweden. *PLoS Med.* **19**, e1004092 (2022).
43. Vogt, N. M. et al. Gut microbiome alterations in Alzheimer's disease. *Sci. Rep.* **7**, 13537 (2017).
44. Balin, B. J. et al. Identification and localization of *Chlamydia pneumoniae* in the Alzheimer's brain. *Med. Microbiol. Immunol.* **187**, 23–42 (1998).
45. Wu, Y. et al. Toll-like receptor 4 and CD11b expressed on microglia coordinate eradication of *Candida albicans*cerebral mycosis. *Cell Rep.* **42**, 113240 (2023).
46. Moné, Y. et al. Evidence supportive of a bacterial component in the etiology for Alzheimer's disease and for a temporal-spatial development of a pathogenic microbiome in the brain. *Front. Cell. Infect. Microbiol.* **13**, 1123228 (2023).
47. Harrison, M. A. A. et al. Intermittent cytomegalovirus infection alters neurobiological metabolism and induces cognitive deficits in mice. *Brain Behav. Immun.* **117**, 36–50 (2024).
48. Itzhaki, R. F. et al. Herpes simplex virus type 1 in brain and risk of Alzheimer's disease. *Lancet* **349**, 241–244 (1997).
49. Saravanan, R. & Bhattacharjya, S. Oligomeric structure of a cathelicidin antimicrobial peptide in dodecylphosphocholine micelle determined by NMR spectroscopy. *Biochim. Biophys. Acta* **1808**, 369–381 (2011).
50. Boman, H. G. Peptide antibiotics and their role in innate immunity. *Annu. Rev. Immunol.* **13**, 61–92 (1995).
51. Teuton, J. R. & Brandt, C. R. Sialic acid on herpes simplex virus type 1 envelope glycoproteins is required for efficient infection of cells. *J. Virol.* **81**, 3731–3739 (2007).
52. Powell-Doherty, R. D., Abbott, A. R. N., Nelson, L. A. & Bertke, A. S. Amyloid-β and p-tau anti-threat response to herpes simplex virus 1 infection in primary adult murine hippocampal neurons. *J. Virol.* **94**, e01874-19 (2020).
53. Luxton, G. W. G. et al. Targeting of herpesvirus capsid transport in axons is coupled to association with specific sets of tegument proteins. *Proc. Natl Acad. Sci. USA* **102**, 5832–5837 (2005).
54. Vittone, V. et al. Determination of interactions between tegument proteins of herpes simplex virus type 1. *J. Virol.* **79**, 9566–9571 (2005).
55. Zambrano, Á et al. Neuronal cytoskeletal dynamic modification and neurodegeneration induced by infection with herpes simplex virus type 1. *J. Alzheimers Dis.* **14**, 259–269 (2008).
56. Johnson, A. M. & Lukens, J. R. The innate immune response in tauopathies. *Eur. J. Immunol.* **53**, e2250266 (2023).
57. Kotsakis, A., Pomeranz, L. E., Blouin, A. & Blaho, J. A. Microtubule reorganization during herpes simplex virus type 1 infection facilitates the nuclear localization of VP22, a major virion tegument protein. *J. Virol.* **75**, 8697 (2001).
58. Kespichayawattana, W., Rattanachetkul, S., Wanun, T., Utaisincharoen, P. & Sirisinha, S. *Burkholderia pseudomallei* induces cell fusion and actin-associated membrane protrusion: a possible mechanism for cell-to-cell spreading. *Infect. Immun.* **68**, 5377–5384 (2000).
59. Sainz, B. & Halford, W. P. Alpha/beta interferon and gamma interferon synergize to inhibit the replication of herpes simplex virus type 1. *J. Virol.* **76**, 11541–11550 (2002).
60. Danastas, K. et al. Interferon inhibits the release of herpes simplex virus-1 from the axons of sensory neurons. *mBio* **14**, e01818-23 (2023).
61. Bigley, N. J. Complexity of interferon-γ interactions with HSV-1. *Front. Immunol.* **5**, 15 (2014).

62. Utech, M. et al. Mechanism of IFN-γ-induced endocytosis of tight junction proteins: myosin II-dependent vacuolarization of the apical plasma membrane. *Mol. Biol. Cell* **16**, 5040–5052 (2005).
63. Wang, Y. et al. The release and trans-synaptic transmission of Tau via exosomes. *Mol. Neurodegener.* **12**, 5 (2017).
64. Dujardin, S. et al. Neuron-to-neuron wild-type Tau protein transfer through a trans-synaptic mechanism: relevance to sporadic tauopathies. *Acta Neuropathol. Commun.* **2**, 14 (2014).
65. Karch, C. M., Jeng, A. T. & Goate, A. M. Extracellular Tau levels are influenced by variability in Tau that is associated with tauopathies. *J. Biol. Chem.* **287**, 42751–42762 (2012).
66. Brunello, C. A., Merezhko, M., Uronen, R.-L. & Huttunen, H. J. Mechanisms of secretion and spreading of pathological tau protein. *Cell. Mol. Life Sci.* **77**, 1721 (2020).
67. Guo, J. L. & Lee, V. M. Y. Cell-to-cell transmission of pathogenic proteins in neurodegenerative diseases. *Nat. Med.* **20**, 130–138 (2014).
68. Ayers, J. I., Giasson, B. I. & Borchelt, D. R. Prion-like spreading in tauopathies. *Biol. Psychiatry* **83**, 337–346 (2018).
69. Liu, S. et al. Reactivated endogenous retroviruses promote protein aggregate spreading. *Nat. Commun.* **14**, 5034 (2023).
70. Ribes, S. et al. Toll-like receptor prestimulation increases phagocytosis of *Escherichia coli*DH5α and *Escherichia coli*K1 strains by murine microglial cells. *Infect. Immun.* **77**, 557–564 (2009).
71. Fekete, R. et al. Microglia control the spread of neurotropic virus infection via P2Y12 signalling and recruit monocytes through P2Y12-independent mechanisms. *Acta Neuropathol.* **136**, 461–482 (2018).
72. Mookherjee, N. et al. Intracellular receptor for human host defense peptide LL-37 in monocytes. *J. Immunol.* **183**, 2688–2696 (2009).
73. Lahaye, X. et al. NONO detects the nuclear HIV capsid to promote cGAS-mediated innate immune activation. *Cell* **175**, 488–501 (2018).
74. Sündermann, F., Fernandez, M.-P. & Morgan, R. O. An evolutionary roadmap to the microtubule-associated protein MAP Tau. *BMC Genomics* **17**, 264 (2016).
75. Moir, R. D. & Tanzi, R. E. low evolutionary selection pressure in senescence does not explain the persistence of Aβ in the vertebrate genome. *Front. Aging Neurosci.* **11**, 70 (2019).

Methods

3D human neuronal cell culture model + microglia

GFP-expressing ReNcell VM neuronal cell line G10, previously described[76], was seeded as a 3D culture in a 96-well plate (Greiner Bio-One, 655866) in ReN Differentiation Media (ReN Diff). ReN Diff changes were completed twice a week until the plate was 3.5–4 weeks old, at which the neuronal culture is considered mature, fully differentiated and ready for experimentation. The 3D human triculture system including neurons, astrocytes and microglia was previously described[77]. In brief, induced pluripotent stem cells are differentiated into mature microglia over 38 days. Once mature, the microglia were resuspended and added at a 6:1 ratio to the 3D ReNcell VM culture for 24 hours followed by a 24-hour HSV-1 infection. After infection, the wells were washed once with PBS and then fixed with 4% paraformaldehyde (PFA) for 2 hours at 4 °C. Then, the plate was washed three times with PBS and stored in PBS at 4 °C until ready for immunostaining. Plate was first blocked with Doo Block shaking at 4 °C overnight. The next day, primary antibodies anti-IBA1 (Abcam, ab283346) at 1:1,000 and anti-p-tau (PHF1, Albert Einstein College of Medicine) at 1:500 were added and incubated at 4 °C overnight shaking. The next day, the plate was washed five times at 5-minute intervals with TBS-Tween. Fluorescent secondaries anti-rat 405 (Invitrogen, A48268) and anti-mouse 647 (Invitrogen, A32787) were added at 1:500 for a 3-hour incubation at 4 °C shaking. Afterwards, the wells were washed five times for 5 minutes each with TBS-Tween and then stored in PBS. Plates were imaged by fluorescence confocal microscopy (Nikon, A1R-HD25) for microglia (405), neurons (GFP), HSV-1 (RFP) and p-tau (647).

Tau HSV1 plaque assay

Two-dimensional (2D) ReNcell VM cultures were seeded in a 24-well plate (Corning, 3526) precoated with 1:100 Matrigel (Corning, 354234) diluted in cold DMEM F-12 at 300,000 cells per well in ReN Expansion Media (ReN Exp) overnight. The next day, the media were replaced by ReN Diff. At 1 week old, the media were removed and replaced with ReN Diff containing 2N4R GSK-3β p-tau (Abcam, ab269024), 2N3R tau (Abcam, ab72462) or 2N4R tau (Abcam, ab84700) overnight at 37 °C at the following concentrations: 2.5 μg ml^{-1}, 1.25 μg ml^{-1} and 0.625 μg ml^{-1}. ReN Diff alone was used for the control wells. The next day, the media were removed, and ReN Diff containing HSV-1 (diluted to 50–200 plaque-forming units (PFU)) were added to each of the wells and centrifuged (Thermo Fisher Scientific, ST8R centrifuge) at 500*g* for 1 hour at room temperature. The HSV-1 media were removed, and ReN Diff containing 0.36% agarose were added to the wells for an overnight incubation at 37 °C. The next day, the plate was imaged by confocal microscopy (Nikon, A1R-HD25) for viral RFP fluorescent signal. Images were analyzed using Nikon Elements General Analysis 3 (GA3) for viral plaque counts, HSV-1-positive single cells and viral plaque size.

GSK-3β inhibitor and anti-INFγ antibody HSV-1 plaque assays

'Tau HSV-1 plaque assay' methodology was adapted to be performed with combinations of a GSK-3β inhibitor (Tocris Bioscience, 4423) and an anti-INFγ antibody (Invivogen, HIFNG-MAB7-02) in place of the synthetic taus from start to finish including image analysis. GSK-3β inhibitor was used at the following concentrations: 50 μg ml^{-1}, 25 μg ml^{-1} and 12.25 μg ml^{-1}; and anti-INFγ antibody was used at 10 μg ml^{-1} for the overnight incubation. In addition, GSK-3β inhibitor was also mixed in with the agarose in its respective concentrations.

Viral capsid isolation

One-half percent Triton X-100 was added to 900 μl of TNE buffer and 100 μl of HSV-1 to create a virus mix stored at 4 °C for 5 minutes. TNE buffer with 35% sucrose was added to ultracentrifuge tubes (Beckman Coulter, 344059) before adding virus mix and then ultracentrifuged (Beckman Coulter, Optima XPN-100 Ultracentrifuge) at 37,000*g* for 45 minutes at 4 °C. After ultracentrifugation, supernatant was aspirated, and the capsid pellet was resuspended in 200 μl of TNE buffer. Capsid mix was added to TNE buffer with 35% sucrose and ultracentrifuged again at 37,000*g* for 45 minutes at 4 °C. The supernatant was aspirated, and capsid-isolated HSV-1 was resuspended in 200 μl of TNE buffer followed by storage at 4 °C for experimentation.

Virus binding assay

Capsid-isolated HSV-1 or whole virion HSV-1 (5×10^6 PFU per well) in distilled water (50 μl per well) was added to a black polypropylene plate (Greiner Bio-One, 655209) and heat-fixed at 95 °C for 2 hours. After heat-fixing, the plate underwent three TBS washes and then was blocked at room temperature for 1-hour shaking using 4% non-fat dry milk. After blocking, the plate was washed three times with TBS-Tween. Synthetic taus 2N4R GSK-3β p-tau (Abcam, ab269024), 2N3R tau (Abcam, ab72462), 2N4R tau (Abcam, ab84700) or 50/50 mix of 2N3R/2N4R taus were added to appropriate wells and incubated at 37 °C for 1 hour at the following concentrations: 5.0 μg ml^{-1}, 2.5 μg ml^{-1}, 1.25 μg ml^{-1}, 0.625 μg ml^{-1} and 0.3125 μg ml^{-1}. After tau incubation, the plate was washed three times with TBS-Tween and then blocked at room temperature for 1-hour shaking using 10% BSA. After blocking, the plate was washed three times with TBS-Tween followed by the addition of an anti-tau antibody (Agilent Technologies, A0024) at 1:10,000 in 10% BSA (100 μl per well) and incubated at 4 °C overnight shaking. The next day, the plate was washed three times with TBS-Tween followed by addition of an anti-rabbit HRP antibody (Cytiva, NA934-100UL) at 1:1,000 in 10% BSA (100 μl per well) and incubated at room temperature for 1-hour shaking. Afterwards, the plate was washed three times with TBS-Tween before adding SuperSignal ELISA Femto Substrate (Thermo Fisher Scientific, 37075). The plate was immediately read on a BioTek Synergy Neo2 Multi-Mode Reader for chemiluminescent signal.

Competitive inhibitor virus binding assay

'Virus binding assay' methodology was adapted to be performed with anticapsid interference antibodies prior to synthetic tau addition. The initial steps up to 4% non-fat milk block and subsequent TBS-Tween washes remain the same. After the washes, anticapsid interference antibodies anti-VP21/VP22a (Thermo Fisher Scientific, MA5-16798), anti-ICP5 (Virusys Corporation, HA018-100), anti-pUL25 (University of Pittsburgh), anti-pUL48-VP16 (Novus Biologicals, NB206593) or anti-RS1-ICP4 (Abcam, ab6514) were added at stepwise dilutions (0.04, 0.2, 1.0 and 5.0 μg ml^{-1}) to appropriate wells and incubated at 37 °C for 1 hour. The plate was then washed three times with TBS-Tween. 2N4R GSK-3β p-tau (Abcam, ab269024), control scrambled LL-37 or 2N4R GSK-3β p-tau incubated with mannose for 1 hour at room temperature was added to wells and incubated at 37 °C for 15 minutes. Then, the plate was washed three times with TBS-Tween followed by a 10% BSA block at room temperature for 1 hour. A subsequent three-times TBS-Tween wash was performed, and a 10% BSA of anti-tau antibody (Agilent Technologies, A0024) at 1:10,000 was added to each well (100 μl per well) for an overnight incubation at 4 °C shaking. The next day, the plate was washed three times with TBS-Tween, and an anti-rabbit HRP antibody (Cytiva, NA934-100UL) at 1:1,000 in 10% BSA (100 μl per well) was added to each well for a 1-hour room temperature incubation shaking. The plate was washed three times with TBS-Tween before adding SuperSignal ELISA Femto Substrate (Thermo Fisher Scientific, 37075). The plate was immediately read on a BioTek Synergy Neo2 Multi-Mode Reader for chemiluminescent signal.

Viral agglutination and TEM analysis

Sample containing capsid-isolated HSV-1 (10 μl) and 2N4R GSK-3β p-tau (10 μl) was incubated for 2 hours at room temperature before being added (10 μl) onto Formvar/Carbon Support Square Grids (Electron Microscopy Sciences, FCF100-Cu) for 2 minutes. Sample was removed by gently touching the perimeter of the grid with filter paper. The grid was transferred to water droplets for 30 seconds three times.

After washes, the grid was dyed by adding 10 µl of 1% uranyl acetate for 1 minute before removing the dye with filter paper and letting the grid sit at room temperature for 10 minutes to dry. Grids were imaged with a JEOL 1011 electron microscope (JEOL Institute).

Slice TEM analysis

3D ReNcell VM cultures were seeded in a six-well plate at 8 million cells per well in ReN Diff and were aged for 3.5 weeks. The cells were infected with HSV-1 (4.06×10^7 PFU per well) and centrifuged with minimal acceleration and deacceleration (Thermo Fisher Scientific, ST8R centrifuge) at 500*g* for 1 hour at room temperature and then incubated at 37 °C for 24 hours. The next day, the media were removed, and the cells were washed once with PBS followed by initial fixation in 4% PFA on a rotator for 30 minutes. Then, fresh 4% PFA was added, and the cells were incubated at 4 °C overnight. The next day, the cells were washed three times using PBS, scraped and spun at 2,200*g* for 15 minutes. The supernatant was removed, and the pellets were resuspended in PBS to be stored at 4 °C. Pellets were loaded onto grids and stained with anti-p-tau (PHF1) antibody incubated with immunogold particles in accordance with 'Viral agglutination and TEM analysis' methodology.

Electron microscopy was performed in the Microscopy Core of the Center for Systems Biology/Program in Membrane Biology, which is partially supported by an Inflammatory Bowel Disease grant (DK043351) and a Boston Area Diabetes and Endocrinology Research Center (BADERC) award (DK057521).

Total tau and p-tau level MSD

3D ReNcell VM cultures were seeded in a 96-well plate (Greiner Bio-One, 655866) and aged for 3.5–4 weeks. At maturation, half the media was removed from the wells and replaced with ReN Diff containing HSV-1 (6.67×10^5 PFU per µl) at 0.5 µl, 0.25 µl or 0.1 µl per well for 24 hours at 37 °C. The next day, the plate was washed once with cold PBS, and cold Sarkosyl lysis buffer was then added to the wells for a 1-hour incubation at 4 °C rocking. The cells were then scraped and collected in a 96-well polymerase chain reaction (PCR) plate to be stored at −20 °C. The cell lysate was thawed and spun (Thermo Fisher Scientific, ST8R centrifuge) at 2,129*g* for 30 minutes to pellet cellular debris. The supernatant was collected and added to an ultracentrifuge tube (Beckman Coulter, 343778) and spun at 279,000*g* (Beckman Coulter, Optima MAX-XP Ultracentrifuge) for 1 hour to separate insoluble and soluble tau. After ultracentrifugation, the supernatant was collected as soluble tau. The remaining pellet was dissolved using guanine hydrochloride and collected as insoluble tau. Both soluble and insoluble tau were added to a 96-well MSD Multi-Spot Phospho (Thr 231)/Total Tau Assay plate (MSD, K15121D-2) and run according to the manufacturer's instructions. Plates were read on an MSD MESO QuickPlex SQ 120 mm, and the resulting raw data were analyzed using MSD Discovery Workbench.

Proinflammatory cytokine MSD

Media for proinflammatory cytokine concentration determination were collected from 24-well plates preincubated with 1.25 µg ml^{-1} 2N4R GSK-3β p-tau (Abcam, ab269024) for 24 hours with or without 1-hour HSV-1 infection the next day. Conditioned media were added to the 96-well V-PLEX Proinflammatory Panel 1 Human Kit (MSD, K15049D) and run according to the manufacturer's instructions. Plates were read on an MSD MESO QuickPlex SQ120 mm, and the resulting raw data were analyzed using MSD Discovery Workbench.

P-tau and total tau immunofluorescence labeling

3D ReNcell VM cultures were seeded in a 96-well plate (Greiner Bio-One, 655866) and aged for 3.5–4 weeks. At maturation, the plate was infected with 30 µl of replication-deficient HSV-1 virus (3.3×10^6 PFU per µl; Heming et al. 2013) mixed with 6 ml of ReN Diff or HSV-1–RFP fusion virus and incubated at 37 °C for 24 hours. The wells were then washed once with PBS and then fixed with 4% PFA at 4 °C for 2 hours. Afterwards, the plate was PBS washed three times followed by blocking with Doo Block at 4 °C shaking overnight. The next day, the following primary antibodies were added for an overnight 4 °C incubation shaking: anti-total tau (Agilent Technologies, A0024) at 1:1,000, anti-p-taus PHF1 (Albert Einstein College of Medicine, gift) or AT180 (Invitrogen, MN1040) at 1:500 and anti-HSV-1 (Invitrogen, PA5-115473) at 1:1,000 only if the replication-deficient HSV-1 was used. The next day, the plate was washed five times at 5-minute intervals using TBS-Tween, and the following secondary antibodies (1:500) were added for a 3-hour 4 °C incubation shaking: anti-rabbit 405 (Jackson ImmunoResearch, 711-475-152), anti-mouse 647 (Invitrogen, A32787) and anti-rabbit 568 (Invitrogen, A10042) if necessary. Afterwards, another five 5-minute TBS-Tween washes were repeated, and the plate was stored in PBS. Plates were imaged by fluorescence confocal microscopy (Nikon, A1R-HD25) and analyzed using Nikon Elements GA3[78].

Microfluidic immunofluorescence

Polydimethylsiloxane microfluidic devices were designed and produced at the Center for Engineering in Medicine at Massachusetts General Hospital (MGH), as described previously[77]. The devices were precoated for 3 hours with 1:100 Matrigel (Corning, 354234) diluted in cold DMEM F-12. 2D ReNcell VM cultures were seeded at 300,000 cells for the outside chambers and 150,000 cells for the middle chamber. The devices were aged for 3.5 weeks followed by a 48-hour 0.5 µl per well HSV-1 (6.67×10^5 PFU per µl) infection of the left chamber. After a PBS wash, the devices were fixed with 4% PFA for 2 hours at 4 °C. The devices followed the immunostaining 'p-tau and total tau immunofluorescence labeling' methodology with a distinction in antibody use. Instead, the antibodies anti-p-tau at 1:500 (PHF1, Albert Einstein College of Medicine) and anti-total tau at 1:750 (GeneTex, GTX49353) fluorescently labeled with secondaries anti-chicken 405 at 1:2,000 (Jackson ImmunoResearch, 703-475-155) and anti-mouse 647 at 1:1,000 (Invitrogen, A32787) were used. Plates were imaged by fluorescence confocal microscopy (Nikon, A1R-HD25) and analyzed using Nikon Elements GA3.

Azide-tagged proteins

2D ReNcell VM cultures were seeded in a 24-well plate containing 0.1-µm inserts (CELLTREAT, 230634) at approximately 75,000 cells per well. The culture was aged for 1 week in methionine-free media (Sigma-Aldrich, D9785-10L). The inserts were infected with HSV-1 (6.67×10^5 PFU per µl) at 1:250 for 24 hours. Six hours after infection, 50 µM L-azidohomoalanine was added. After infection, the inserts were removed, and the wells were fixed in 4% PFA for 1 hour at room temperature. After three washes of PBS, a permeabilizing solution of 0.5% Triton X-100 PBS was added for 15 minutes at room temperature. After three washes of PBS, a click reaction mix of 50 µM Alexa Fluor 647 Alkyne (Life Technologies, A32787), 100 mM copper sulfate and 1 M dithiothreitol in PBS were added to the wells for 1 hour at room temperature while being protected from light. The wells were then washed three times with PBS, and 5% BSA was added overnight. The next morning, three PBS washes were followed with anti-p-tau (PHF1, Albert Einstein College of Medicine) antibody at 1:500 shaking overnight at 4 °C. After three PBS washes, the plate was stained with secondary anti-mouse 594 (Invitrogen, A11032) at 1:1,000 in 5% BSA. Three more PBS washes were completed, and the wells were stored in PBS. Wells were imaged by confocal microscopy (Nikon, A1R-HD25) and analyzed by Nikon Elements GA3.

Thioflavin S co-localization

3D ReNcell VM cultures seeded in a 96-well plate (Greiner Bio-One, 655866) were aged to 3.5 weeks. At 3.5 weeks, the media were completely removed and replaced with media containing HSV-1 (2.465×10^7 PFU per well) and incubated for 24 hours at 37 °C. The wells were then washed once with PBS and then fixed with 4% PFA PBS at 4 °C for 2 hours.

Afterwards, the plate was PBS washed three times followed by blocking with Doo Block at 4 °C shaking overnight. Then, anti-p-tau (PHF1, Albert Einstein College of Medicine) at 1:500 in Doo Block was added, and the plate was incubated at 4 °C shaking overnight. After overnight incubation, the plates were washed five times at 5- minute intervals using TBS-Tween. Fluorescent secondary anti-mouse 647 (Invitrogen, A32787) was added at 1:1,000 in Doo Block, and the plate was incubated on a shaker for 3 hours at 4 °C. Five 5-minute washes were repeated, and then 0.05% thioflavin S dissolved in 50% ethanol/water was added to the wells for 10 minutes. This was followed by three 80% ethanol/water washes and seven PBS washes for 10-minute intervals. After the final wash, the plates were stored in PBS at 4 °C. Plates were imaged by fluorescence confocal microscopy (Nikon, A1R-HD25), and images were analyzed using Nikon Elements GA3.

Cytoxicity assay

Three and one-half to four-week-old 3D ReNcell VM cultures were infected with serial dilutions of HSV-1 for 24 hours. Conditioned media were collected and stored at −20 °C in LDH storage buffer. The samples were later analyzed using an LDH-Glo Cytotoxicity Assay (Promega, J2381), and luminescence values were recorded from a plate reader (BioTek Synergy Neo2).

Statistics and reproducibility

Statistical parameters, tests used, sample sizes and number of repeats are noted in the figure legends. No statistical methods were used to predetermine sample sizes; sample sizes were chosen based on previous similar studies[10,11]. Data collection was randomized. Data collection and analysis were performed blinded to the conditions of the experiments whenever possible—however, not for all experiments. Exclusion of data points was performed based on standard GraphPad Prism outlier analysis (ROUT method, $Q = 1\%$). Images are representative of all experimental repeats. Statistical significance between two groups was determined using two-tailed Student's *t*-tests, or, in cases where assumptions of normal distribution or variance are violated, Mann–Whitney test or Welch's *t*-test was used, respectively. Statistical significance for more than two groups was determined with multiple comparison ANOVAs. In cases where normal distribution assumptions were violated, a normality test was performed, and the subsequent significance test was determined accordingly. Comparisons between treatment groups only to a single control group were corrected using Dunnett's correction. Comparisons between all groups were corrected using Tukey's correction. In several instances, multiple independent comparisons were corrected using Sidak's correction. Linear regression analyses were used to determine a rate of constancy between two quantitative variables. In several instances, Kolmogorov–Smirnov test was used to determine cumulative distribution function between two independent samples. All images from in vitro samples are representative of multiple image fields described in each figure legend from a minimum of three independent experiments. The threshold for determining statistical significance was $P < 0.05$. All statistical analyses were performed with GraphPad Prism 10.

Reporting summary

Further information on research design is available in the Nature Portfolio Reporting Summary linked to this article.

Data availability

Data underlying Figs. 1, 2 and 4–6 and Extended Data Figs. 1–9 are provided with the paper. Source data are provided with this paper.

Code availability

Nikon NIS Elements General Analysis 3 workflows or 'recipes' for image analysis are available from the corresponding authors upon reasonable request.

References

76. Kim, Y. H. et al. A 3D human neural cell culture system for modeling Alzheimer's disease. *Nat. Protoc.* **10**, 985–1006 (2015).
77. Park, J. et al. A 3D human tri-culture system modeling neurodegeneration and neuroinflammation in Alzheimer's disease. *Nat. Neurosci.* **21**, 941–951 (2018).
78. Heming, J. D., Huffman. J. B., Jones, L. M. & Homa, F. L. Isolation and characterization of the herpes simplex virus 1 terminase complex. *J. Virol.* https://doi.org/10.1128/JVI.02632 (2014).

Acknowledgements

We would like to acknowledge the support given by the National Institute of Aging (RF1AG061035-01 to R.D.M.) and the Cure Alzheimer's Fund (W.A.E. and R.E.T.). The funders had no role in study design, data collection and analysis, decision to publish or preparation of the manuscript. The authors thank D. Irimia and the BioMEMS Core at MGH for assistance with microfluidic device design and production. We also thank D. Capen and the MGH PMB Microscopy Core Facility for technical assistance with electron microscopy.

Author contributions

W.A.E., R.D.M. and R.E.T. conceived the hypothesis and strategies for this project. W.A.E. and R.E.T. supervised the project. W.A.E., D.K.K., N.K.S. and R.E.T. contributed to experimental design. W.A.E., A.S.R., M.T.D., S.E., S.S. and T.S. carried out experiments and data analysis. J.P. helped design and supervise the utilization of 3D neuronal cultures and microglial experiments. W.A.E. wrote the manuscript, with help from A.S.R. and M.T.D. All authors contributed to manuscript editing.

Competing interests

The authors declare no competing interests.

Additional information

Extended data is available for this paper at https://doi.org/10.1038/s41593-025-02157-0.

Supplementary information The online version contains supplementary material available at https://doi.org/10.1038/s41593-025-02157-0.

Correspondence and requests for materials should be addressed to William A. Eimer or Rudolph E. Tanzi.

Peer review information *Nature Neuroscience* thanks the anonymous reviewer(s) for their contribution to the peer review of this work.

https://doi.org/10.1038/s41593-025-02157-0

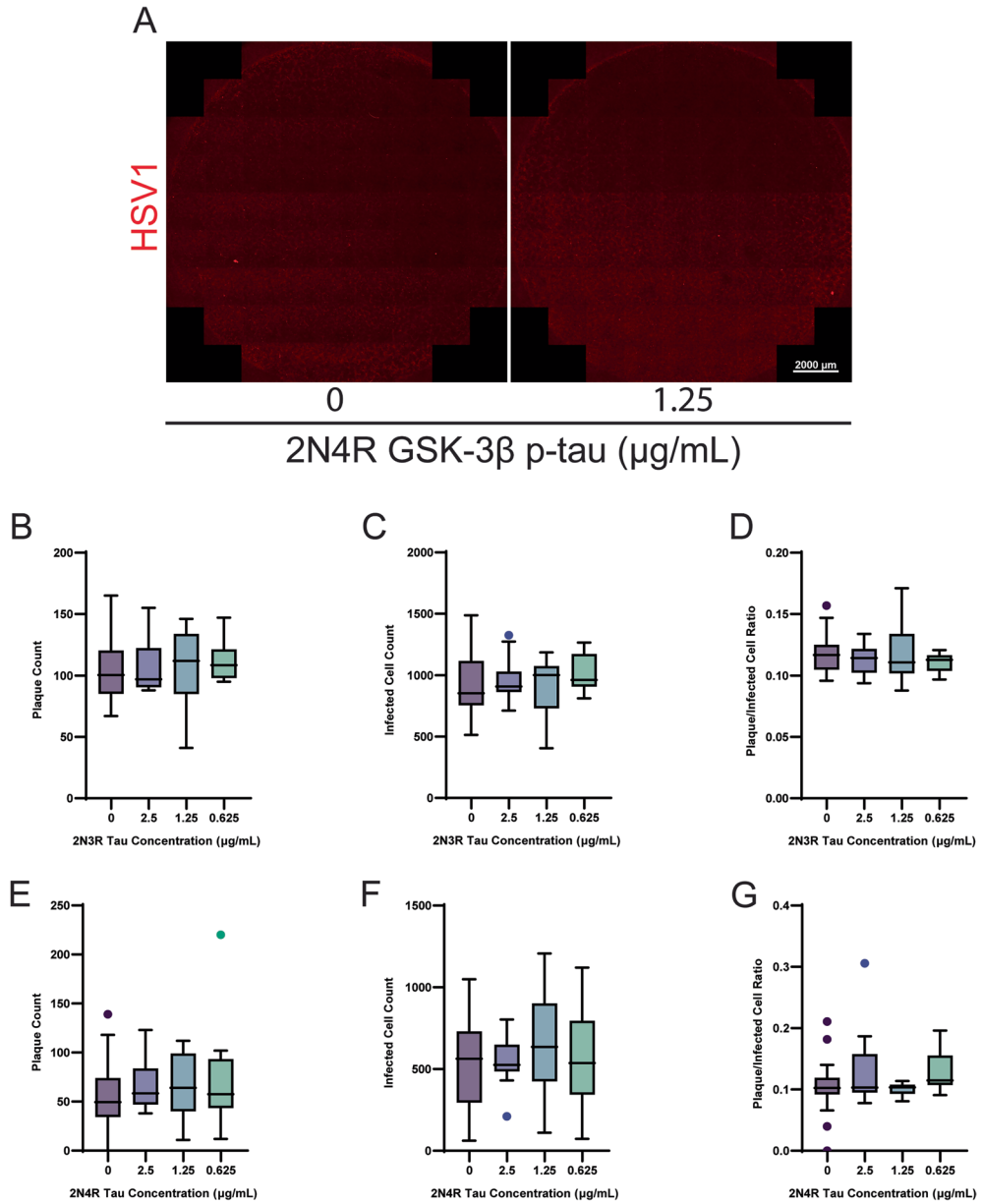

Extended Data Fig. 1 | GSK-3β treated 2N4R tau, but not non-phosphorylated tau, reduces HSV1 plaque formation in human cell culture model. 2D ReNcell VM cultures were pre-incubated with dilutions of synthetic 2N3R tau, 2N4R tau, or 2N4R GSK-3β phosphorylated tau (p-tau) followed by infection with HSV1 to assay tau's antimicrobial protective properties. After HSV1 infection, whole wells were imaged by confocal microscopy and analyzed for red fluorescence. (**a**) Whole well images comparing HSV1 plaque formation in the absence or presence of 2N4R GSK-3β p-tau (1.25 µg/mL). (**b-g**) Whole well images from the 2N3R or 2N4R tau pre-treated conditions (scale of 2.5 to 0.625 µg/mL) were analyzed using Nikon Elements GA3 Analysis to compare (**b, e**) the number of HSV1 plaques, (**c, f**) the number of HSV1 single cell infections, and (**d, g**) the ratio of plaques to single cell infections. Box plots are representative of ±SEM ([B-D, n=11], [E-G, n=12]) depicting median and IQR with whiskers denoting variability according to Tukey's method. Statistical mean comparisons were calculated by one-way ANOVA using Dunnett's multiple comparison test (**b-f**).

https://doi.org/10.1038/s41593-025-02157-0

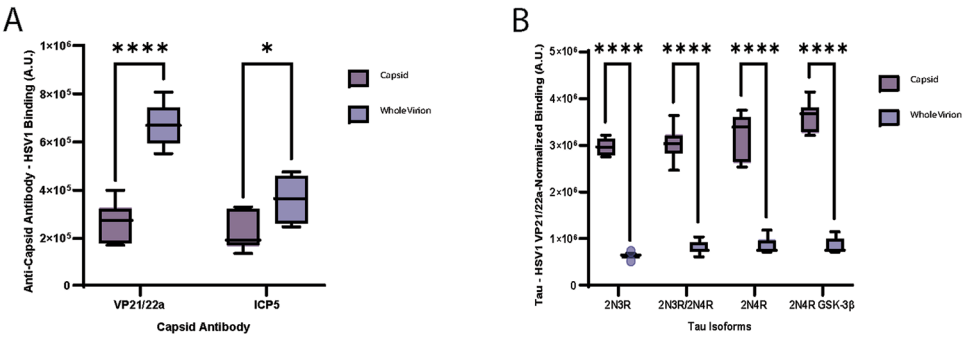

Extended Data Fig. 2 | Anti-capsid antibodies and tau isoforms have a higher binding affinity to HSV1 capsid than whole virion. Anti-capsid antibodies and synthetic tau isoforms were incubated with heat-immobilized HSV1 capsid or whole virion in an indirect ELISA to measure tau-virus binding affinity differences between isolated viral capsids and whole virions with intact envelopes. (**a**) Anti-capsid antibodies VP21/22a and ICP5 viral binding were compared between isolated HSV1 capsids and whole virion ($F_{(1, 20)}$=14.29, **P*=0.0136, *****P*<0.0001). (**b**) Synthetic tau isoforms 2N3R, 50/50 mix of 2N3R/2N4R, 2N4R, and synthetic 2N4R GSK-3β p-tau binding affinities were compared between isolated HSV1 capsids and whole virion normalized against VP21/22a antibody binding ($F_{(3, 88)}$=4.957, *****P*<0.0001). Box plots are representative of ±SEM ([A, n=6], [B, n=12]) depicting median and IQR with whiskers denoting variability according to Tukey's method. Statistical significance was calculated by two-way ANOVA using Šídák's multiple comparisons test (**a, b**).

https://doi.org/10.1038/s41593-025-02157-0

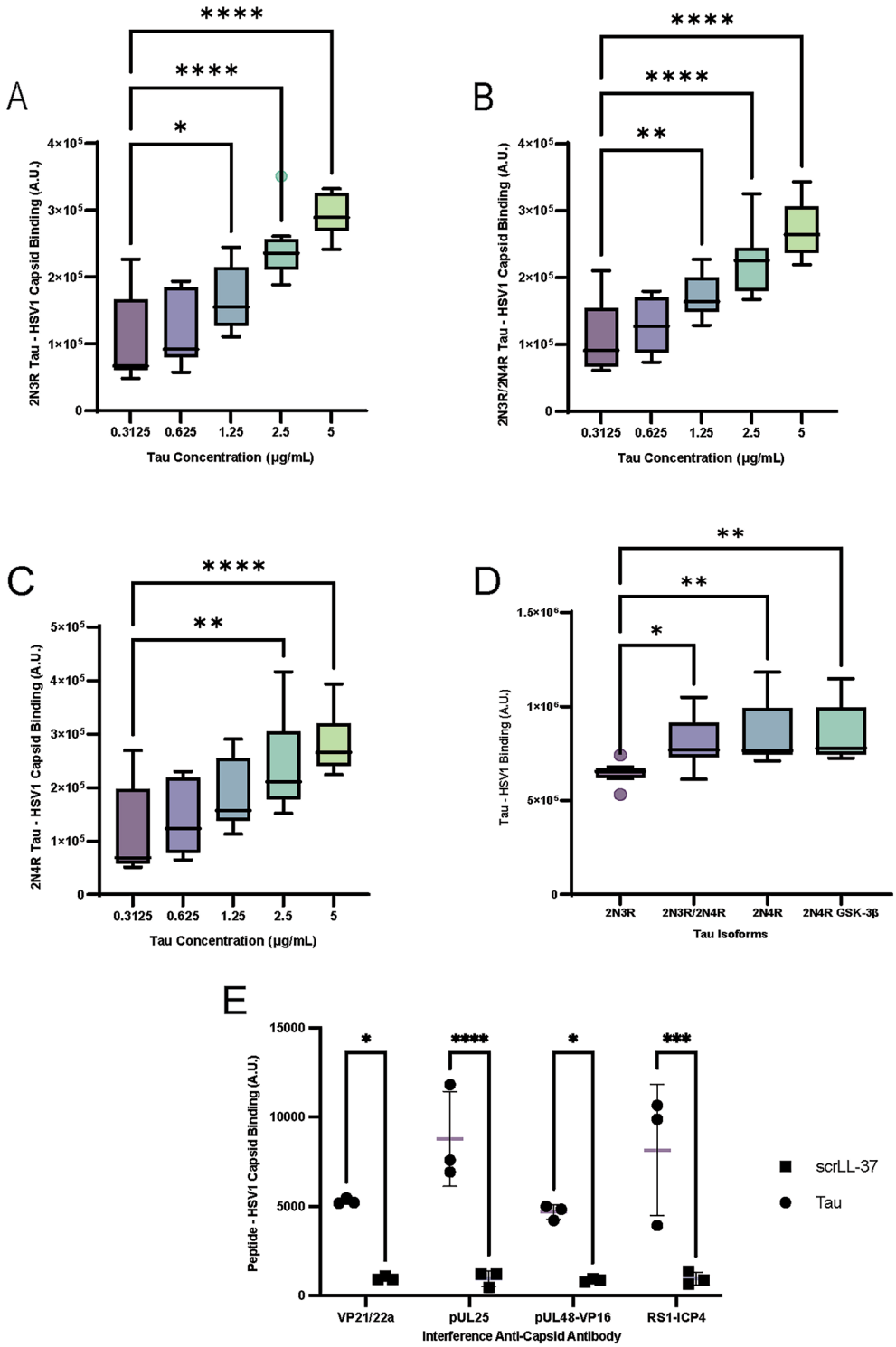

Extended Data Fig. 3 | 2N3R tau isoform has the lowest binding affinity to HSV1 compared to other tau isoforms. Dilutions of synthetic tau isoforms were incubated with heat-immobilized HSV1 capsid or whole virion in an indirect ELISA to measure tau-virus binding affinity. (**a**) Dilutions of 2N3R tau (scale of 5 to 0.3125 µg/mL) are incubated with immobilized HSV1 capsids ($F_{(4,55)}$=33.42, **P*=0.0232, *****P*<0.0001). (**b**) Dilutions of a 50/50 mixture of 2N3R/2N4R tau (scale of 5 to 0.3125 µg/mL) are incubated with immobilized HSV1 capsids ($F_{(4,55)}$= 30.21, ***P*=0.0071, *****P*<0.0001). (**c**) Dilutions of 2N4R tau (scale of 5 to 0.3125 µg/mL) are incubated with immobilized HSV1 capsids ($F_{(4,55)}$=11.50, ***P*=0.0011, *****P*<0.0001). (**d**) 2N4R GSK-3β p-tau binding to HSV1 was compared to 2N3R, 50/50 mix of 2N3R/2N4R, and 2N4R tau ($F_{(3,44)}$=6.913, **P*=0.0211, [2N4R tau vs. 2N3R tau, ***P*=0.0025], [2N4R GSK-3β p-tau vs. 2N3R tau, ***P*=0.0012]) (**e**) 2N4R GSK-3β p-tau and scrambled-sequence LL-37 are incubated with immobilized HSV1 capsids ($F_{(3,16)}$=2.299, **P*=0.0422, ****P*=0.0002, *****P*<0.0001). Box plots are representative of ±SEM (n=12) depicting median and IQR with whiskers denoting variability according to Tukey's method. Statistical significance was calculated by one-way ANOVA using Tukey's multiple comparisons test (**a-d**) and two-way ANOVA using Šídák's multiple comparisons test (**e**).

https://doi.org/10.1038/s41593-025-02157-0

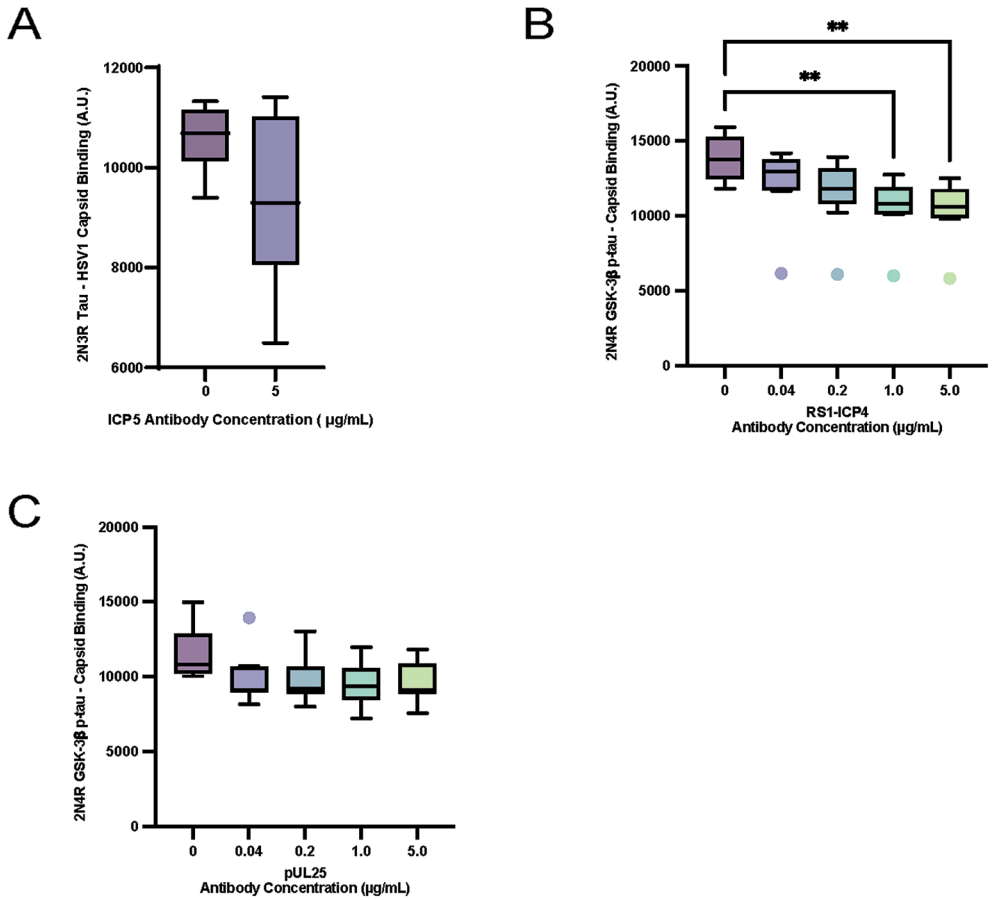

Extended Data Fig. 4 | Site-specific anti-capsid antibodies less effectively inhibit tau binding to HSV1. Synthetic 2N3R tau and 2N4R GSK-3β p-tau isoforms were incubated with heat-immobilized HSV1 capsid after pre-incubation with anti-capsid protein antibodies in an indirect ELISA to examine inhibition of tau-capsid binding. (**a**) 2N3R tau binding to HSV1 capsid was pretreated with anti-ICP5 antibody. (**b**) 2N4R GSK-3β p-tau binding to HSV1 capsid was pretreated with anti-RS1-ICP4 antibody ($F_{(8, 32)}$=13.59, [0 vs. 1.0 µg/mL, ***P*=0.0064], [0 vs. 5.0 µg/mL, ***P*=0.0056]). (**c**) 2N4R GSK-3β p-tau binding to HSV1 capsid was pretreated with anti-pUL25 antibody. Box plots are representative of ±SEM (n=12) depicting median and IQR with whiskers denoting variability according to Tukey's method. Statistical significance was calculated by two-tailed Mann-Whitney test (**a**) and one-way ANOVA using Dunnett's multiple comparison test (**b, c**).

https://doi.org/10.1038/s41593-025-02157-0

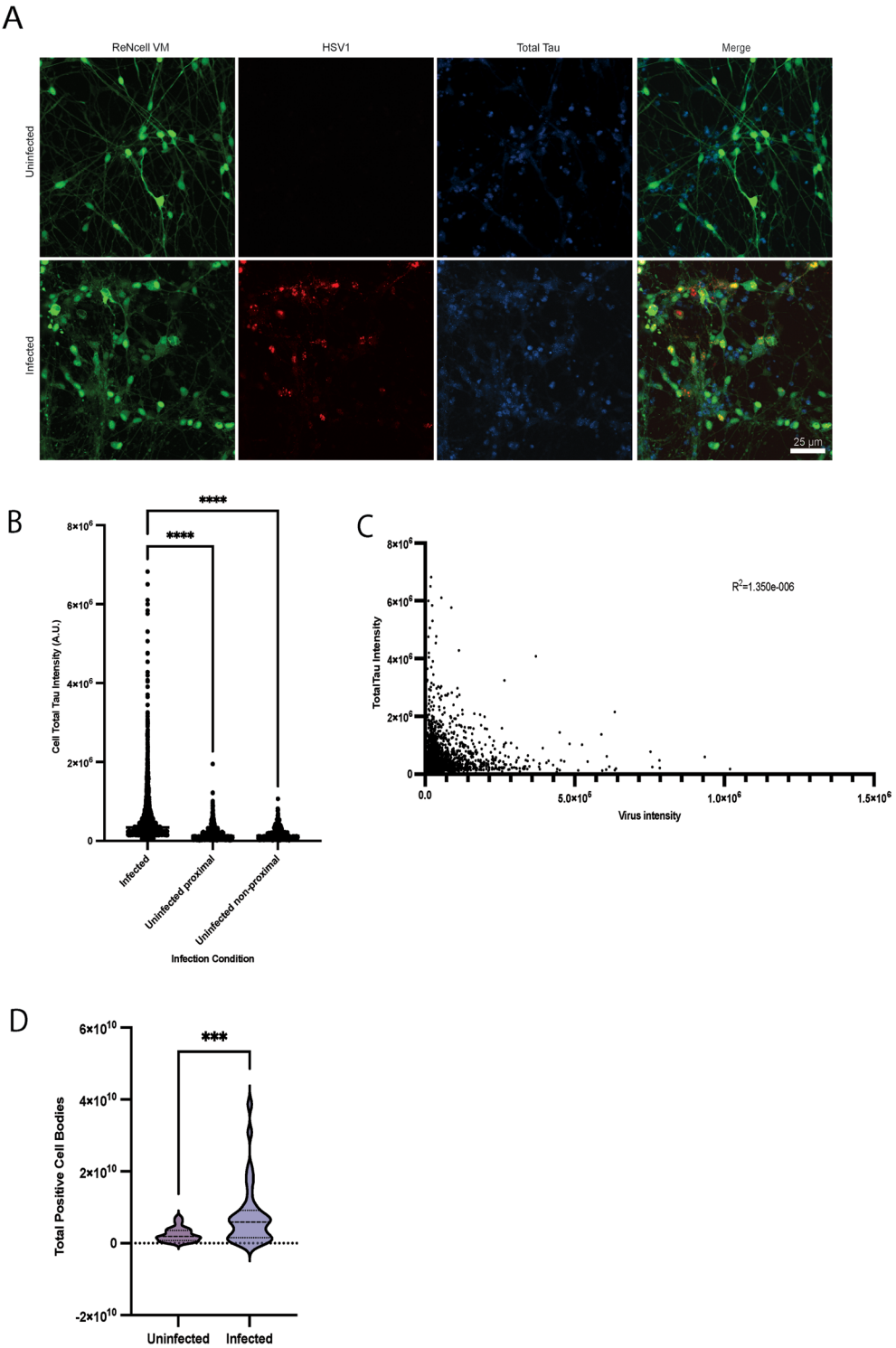

Extended Data Fig. 5 | Cellular total tau fluorescence is increased in HSV1 infected neurons but not in adjacent uninfected neurons. ReNcell VM cultures were infected with HSV1 for 24 hours to characterize total tau's distribution changes from infection and in proximity to viral infection. (**a**) 2D ReNcell VM cultures in microfluidic devices were infected in the left chamber with HSV1 for 48 hours, immunoprobed with anti-total tau labeled with a fluorescent secondary antibody, and analyzed for total tau (405), neurons (GFP), and HSV1 (RFP) fluorescence by confocal microscopy. Fluorescence signals were compared by General Analysis 3 (GA3). (**b**) GA3 of HSV1-positive neurons compared intracellular p-tau fluorescence between infected neurons, uninfected neurons proximal to infected neurons, and uninfected neurons not proximal to infected neurons ($F_{(2, 3321)}$=166.3, ****P<0.0001). (**c**) Individual neuronal total tau fluorescent intensity was compared to total proximal HSV1-RFP fluorescent intensity (R^2=1.350e-006). (**d**) Fluorescent image captures from 384 wells over 4 experiments were compared for total tau fluorescence in cell bodies (***P=0.0003) between uninfected and infected wells. Statistical mean comparisons were calculated by one-way ANOVA (**b**), simple linear regression (**c**), and two-tailed paired t-test (**d**). Images are representative of experiments repeated in triplicate.

https://doi.org/10.1038/s41593-025-02157-0

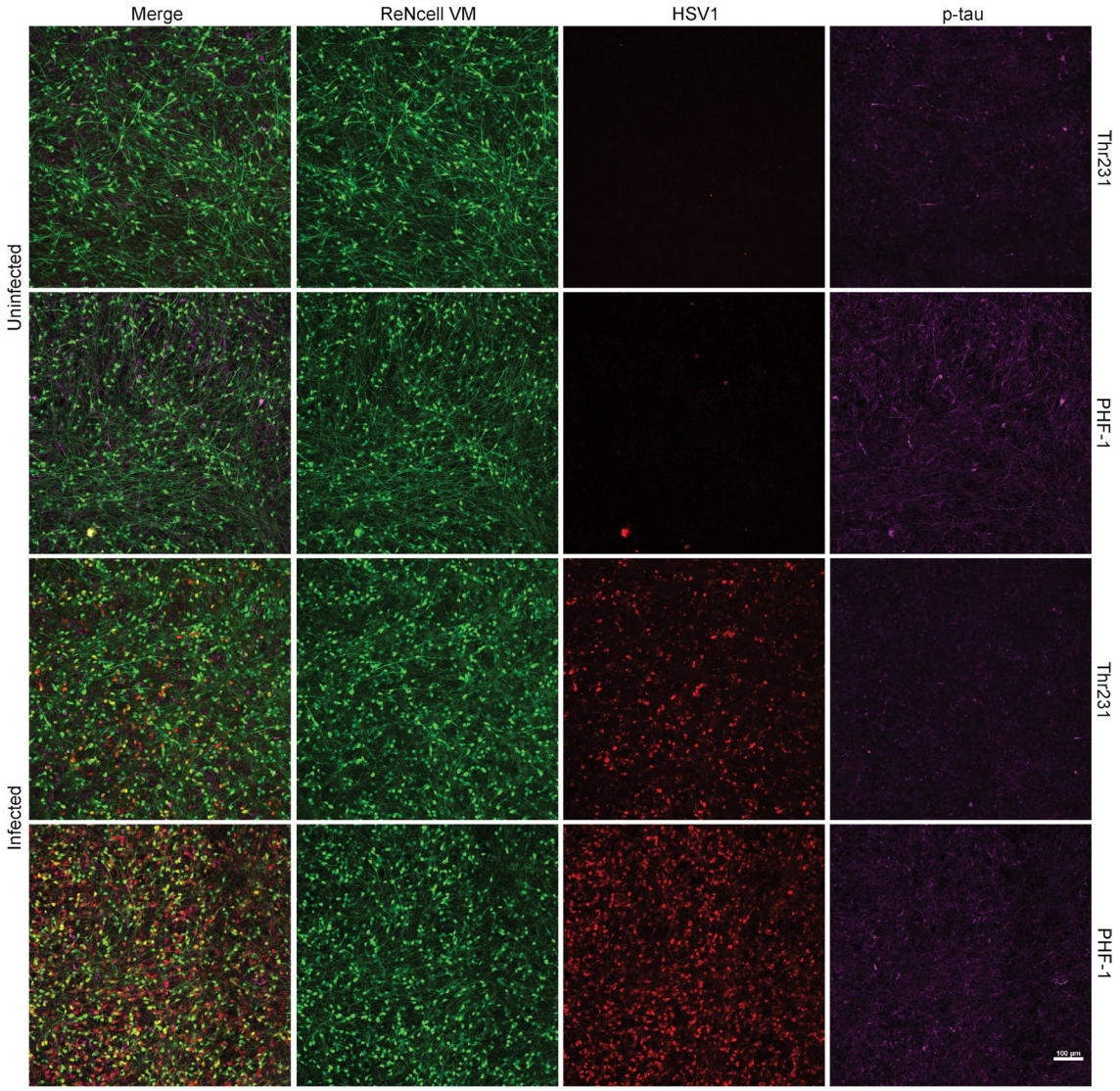

Extended Data Fig. 6 | The phosphorylation of tau from an HSV1 infection occurs at multiple phosphorylation sites. 3D ReNcell VM cultures were infected with HSV1 to characterize tau's change in cellular distribution and levels to viral infection. 96 well plates were immunoprobed with anti-p-tau antibodies AT180 and PHF-1 labeled with a fluorescent secondary antibody. Images were collected via confocal microscopy and immunofluorescent representative images show neurons (GFP), HSV1 (RFP), and p-tau (647). Images are representative of experiments repeated in triplicate.

https://doi.org/10.1038/s41593-025-02157-0

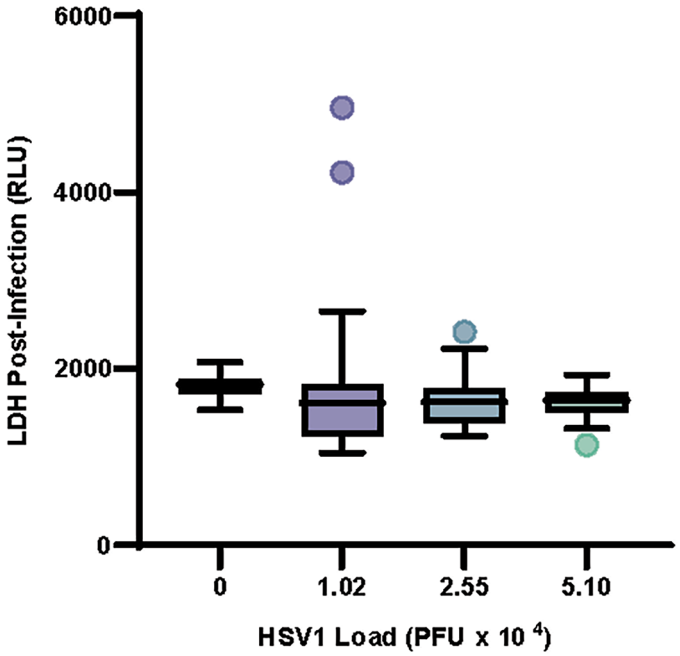

Extended Data Fig. 7 | Cell death is not increased by HSV1 24 hours post infection. Conditioned media from 24 hour HSV1 infected 3D ReNcell VM cultures were analyzed via a cytotoxicity assay to characterize culture cell death. Box plots are representative of ±SEM (n=30) depicting median and IQR with whiskers denoting variability according to Tukey's method. Statistical significance was calculated by one-way ANOVA using Dunnett's multiple comparison test.

https://doi.org/10.1038/s41593-025-02157-0

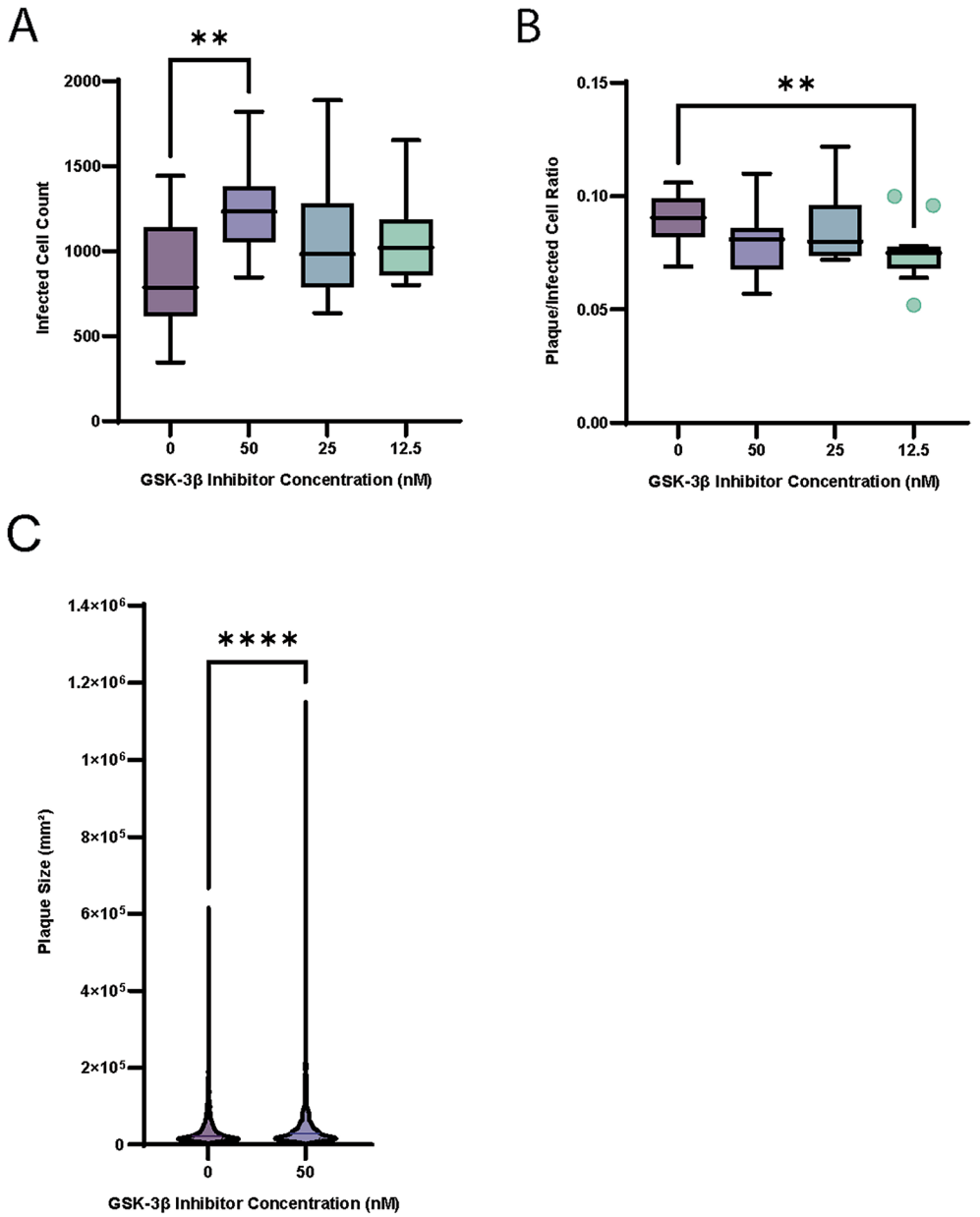

Extended Data Fig. 8 | HSV1 infectivity and plaque sizes increase following progressive GSK-3β inhibition. 1 week old 2D ReNcell VM cultures were pre-incubated with a GSK-3β inhibitor for 24 hours followed by a 24 hour HSV1 infection to assess reduced kinase activity on viral replication. Post-infection whole wells were imaged by confocal microscopy and analyzed for red fluorescence. Images were analyzed using Nikon Elements GA3 Analysis to compare (**a**) the number of HSV1 single cell infections ($F_{(3,53)}$=5.204, $^{**}P$=0.0012), (**b**) the ratio of plaques to single cell infections ($F_{(3,53)}$=4.173, $^{**}P$=0.0046), and (**c**) the size of individual HSV1 plaques by area ($^{****}P$<0.0001). Bars represent the distribution of replicate wells (n=11), with whiskers denoting variability according to Tukey's method. Statistical mean comparisons were calculated by one-way ANOVA using Dunnett's multiple comparisons test (**a, b**) and two-tailed Kolmogorov-Smirnov test (**c**).

https://doi.org/10.1038/s41593-025-02157-0

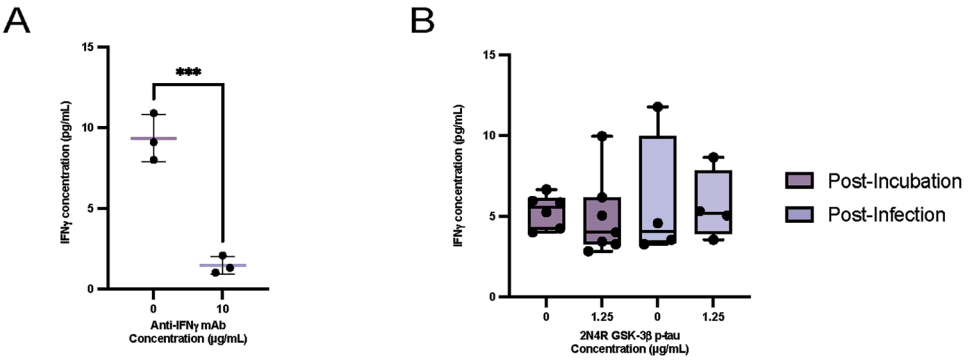

Extended Data Fig. 9 | IFNγ concentration is effectively reduced by neutralizing anti-IFNγ antibodies, but is not altered by p-tau pre-incubation. 2D ReNcell VM cultures were pre-incubated with 2N4R GSK-3β p-tau or an IFNγ antibody followed by a short-term HSV1 infection to observe effects on extracellular IFNγ levels. (**a**) IFNγ concentrations in conditioned media were measured following a 24 hour pre-incubation of IFNγ antibody and again following HSV1 infection. ($F_{(2,2)}$=7.093, P^{***}<0.0010). (**b**) IFNγ concentrations in conditioned media were measured following a 24 h pre-incubation of 2N4R GSK-3β p-tau and again following HSV1 infection. Box plots are representative of ±SEM ([A, n=3], [B, n=4]) depicting median and IQR with whiskers denoting variability according to Tukey's method. Statistical mean comparison was calculated by two-tailed unpaired t-test (**a**) and two-tailed Welch's t-test (**b**).

https://doi.org/10.1038/s41593-025-02157-0

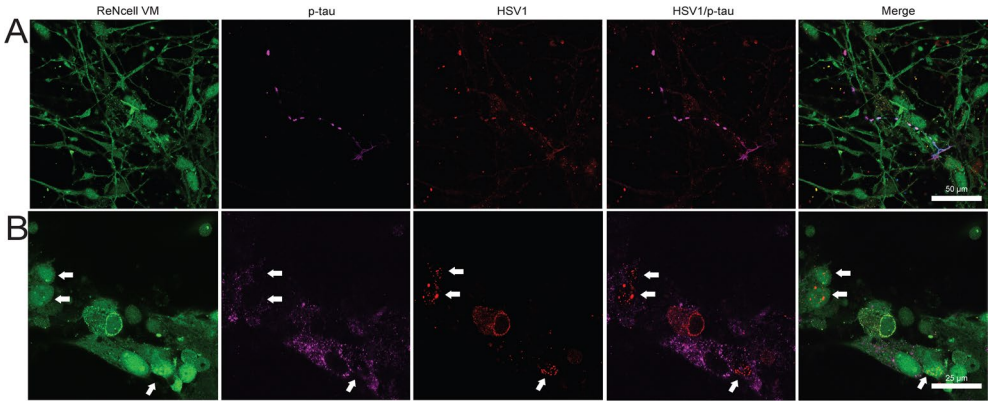

Extended Data Fig. 10 | p-tau localizes in dystrophic neurites with HSV1 and around infected nuclei during viral replication. 3D ReNcell VM cultures were infected with HSV1 to characterize tau's co-localization with HSV1. (**a, b**) 3D ReNcell VM cultures were infected with HSV1 for 24 h, immunoprobed with anti-p-tau (PHF-1) labeled with a fluorescent secondary antibody, and analyzed for neurons (GFP), HSV1 (RFP), and p-tau (647) fluorescence by confocal microscopy. (**a**) Dystrophic neurites, identified by punctate linear formations originating from a cell soma, contain p-tau and HSV1 fluorescence. (**b**) Increased punctate p-tau fluorescence observed in neuron soma adjacent to HSV1-positive cells and in cells with nuclear replication compartments (arrows). Panels are representative of data from multiple discrete imaging fields across experiments repeated in triplicate.

nature portfolio

Corresponding author(s): Rudolph Tanzi, William Eimer

Last updated by author(s): Oct 24, 2025

Reporting Summary

Nature Portfolio wishes to improve the reproducibility of the work that we publish. This form provides structure for consistency and transparency in reporting. For further information on Nature Portfolio policies, see our Editorial Policies and the Editorial Policy Checklist.

Statistics

For all statistical analyses, confirm that the following items are present in the figure legend, table legend, main text, or Methods section.

n/a	Confirmed
☐	☒ The exact sample size (*n*) for each experimental group/condition, given as a discrete number and unit of measurement
☐	☒ A statement on whether measurements were taken from distinct samples or whether the same sample was measured repeatedly
☐	☒ The statistical test(s) used AND whether they are one- or two-sided *Only common tests should be described solely by name; describe more complex techniques in the Methods section.*
☐	☒ A description of all covariates tested
☐	☒ A description of any assumptions or corrections, such as tests of normality and adjustment for multiple comparisons
☐	☒ A full description of the statistical parameters including central tendency (e.g. means) or other basic estimates (e.g. regression coefficient) AND variation (e.g. standard deviation) or associated estimates of uncertainty (e.g. confidence intervals)
☐	☒ For null hypothesis testing, the test statistic (e.g. *F*, *t*, *r*) with confidence intervals, effect sizes, degrees of freedom and *P* value noted *Give P values as exact values whenever suitable.*
☒	☐ For Bayesian analysis, information on the choice of priors and Markov chain Monte Carlo settings
☒	☐ For hierarchical and complex designs, identification of the appropriate level for tests and full reporting of outcomes
☐	☒ Estimates of effect sizes (e.g. Cohen's *d*, Pearson's *r*), indicating how they were calculated

Our web collection on statistics for biologists contains articles on many of the points above.

Software and code

Policy information about availability of computer code

Data collection	Nikon Elements AR v.5.21.03
Data analysis	Nikon Elements AR v.5.21.03, Graphpad Prism v 10.0

For manuscripts utilizing custom algorithms or software that are central to the research but not yet described in published literature, software must be made available to editors and reviewers. We strongly encourage code deposition in a community repository (e.g. GitHub). See the Nature Portfolio guidelines for submitting code & software for further information.

Data

Policy information about availability of data

All manuscripts must include a data availability statement. This statement should provide the following information, where applicable:

- Accession codes, unique identifiers, or web links for publicly available datasets
- A description of any restrictions on data availability
- For clinical datasets or third party data, please ensure that the statement adheres to our policy

Source data for Figures 1, 2, 4-6, and Extended Data Figures 1-9 are provided with the paper. Any further data that support the findings of this study are available from the corresponding author upon request.

Research involving human participants, their data, or biological material

Policy information about studies with human participants or human data. See also policy information about sex, gender (identity/presentation), and sexual orientation and race, ethnicity and racism.

Reporting on sex and gender	N/A
Reporting on race, ethnicity, or other socially relevant groupings	N/A
Population characteristics	N/A
Recruitment	N/A
Ethics oversight	N/A

Note that full information on the approval of the study protocol must also be provided in the manuscript.

Field-specific reporting

Please select the one below that is the best fit for your research. If you are not sure, read the appropriate sections before making your selection.

☒ Life sciences ☐ Behavioural & social sciences ☐ Ecological, evolutionary & environmental sciences

For a reference copy of the document with all sections, see nature.com/documents/nr-reporting-summary-flat.pdf

Life sciences study design

All studies must disclose on these points even when the disclosure is negative.

Sample size	Samples sizes were based on previous published experimental procedures. For new procedures, optimization trials were run to determine necessary sample size. (Eimer et al., 2018 and Kumar et al., 2016)
Data exclusions	Outliers were identified using the ROUT method in GraphPad Prism and excluded from final analyses.
Replication	All experiments with statistics were replicated at least three times, each time in triplicate. For experiments that were not quantified (ICC), a minimal of three separate cultures were imaged and confirmed to have matching morphology.
Randomization	Randomization was conducted where possible. Controls were performed with each iteration of experiments to account for experimental variation and allow for data normalization.
Blinding	Investigators were blinded for data collection and analysis when possible. Most experiments with negative infection controls could not be blinded due to viral tagging. All quantification was carried out agnostically with computer assisted analysis applied across all conditions to eliminate bias.

Reporting for specific materials, systems and methods

We require information from authors about some types of materials, experimental systems and methods used in many studies. Here, indicate whether each material, system or method listed is relevant to your study. If you are not sure if a list item applies to your research, read the appropriate section before selecting a response.

Materials & experimental systems

n/a	Involved in the study
☐	☒ Antibodies
☐	☒ Eukaryotic cell lines
☒	☐ Palaeontology and archaeology
☒	☐ Animals and other organisms
☒	☐ Clinical data
☒	☐ Dual use research of concern
☒	☐ Plants

Methods

n/a	Involved in the study
☒	☐ ChIP-seq
☒	☐ Flow cytometry
☒	☐ MRI-based neuroimaging

Antibodies

Antibodies used

Primary antibodies:
1) Anti-total-tau Genetex GTX49353. For IF - 1:750
https://www.citeab.com/antibodies/3843065-gtx49353-tau-antibody?des=37dc0705dd718164
2) Anti-p-tau PHF1 Albert Einstein College of Medicine. For IF - 1:500
https://www.nature.com/articles/nprot.2015.065
3) Anti-p-tau (AT180) Invitrogen MN1040. For IF - 1:500
https://www.thermofisher.com/antibody/product/Phospho-Tau-Thr231-Antibody-clone-AT180-Monoclonal/MN1040
4) Anti-total tau (Dako) Agilent A0024. For ELISA - 1:10000. For IF - 1:1000
https://www.citeab.com/antibodies/3382933-a0024-tau
5) Anti-HSV1-VP21/VP22a (LP13) Invitrogen MA5-16798. For ELISA - 0.04, 0.2, 1.0, 5.0 µg/mL
https://www.thermofisher.com/antibody/product/HSV-Type-1-VP21-VP22a-Antibody-clone-LP13-Monoclonal/MA5-16798
6) Anti-HSV1-ICP5 Virusys Corporation HA018-100. For ELISA - 0.04, 0.2, 1.0, 5.0 µg/mL
https://www.antibodyregistry.org/AB_2713935
7) Anti-HSV1-pUL25 Homa Lab University of Pittsburgh. For ELISA - 0.04, 0.2, 1.0, 5.0 µg/mL
8) Anti-HSV1-pUL48-VP16 Novus Biologicals NB206593. For ELISA - 0.04, 0.2, 1.0, 5.0 µg/mL
9) Anti-HSV1-RS1-ICP4 (10F1) Abcam ab6514. For ELISA - 0.04, 0.2, 1.0, 5.0 µg/mL
https://www.abcam.com/en-us/products/primary-antibodies/hsv-1-icp4-immediate-early-protein-antibody-10f1-ab6514?srsltid=AfmBOoqyYUqtntAL0vC1knr7ylmVbVcVK42FRhW3zNLrb02FRO3hQ1Mp
10) Anti-INFγ antibody Invivogen HIFNG-MAB7-02. For neutralization - 10 µg/mL
11) Anti-HSV1 (strain 17) Invitrogen PA5-115473. For IF - 1:1000
https://www.thermofisher.com/antibody/product/Herpes-Simplex-Virus-Type-1-strain-17-Antibody-Polyclonal/PA5-115473
12) Anti-IBA1 Abcam ab283346. For IF - 1:1000
https://www.abcam.com/en-us/products/primary-antibodies/iba1-antibody-epr16589-microglia-marker-rat-igg2a-chimeric-ab283346?srsltid=AfmBOopLuU6otfbOllz4TQhqQbSgOM0TEF39XdxJqM_Vw27-o0Fev279

Secondary antibodies:
1) Anti-rabbit 405 Jackson Immunoresearch 711-475-152. For IF - 1:500
2) Anti-rat 405 Invitrogen A48268. For IF - 1:500
3) Anti-chicken 405 Jackson Immunoresearch 703-475-155. For IF - 1:2000
4) Anti-rabbit 568 Invitrogen A10042. For IF - 1:500
5) Anti-mouse 594 Invitrogen A11032. For IF - 1:500
6) Anti-mouse 647 Invitrogen A32787. For IF - 1:500
7) Anti-rabbit HRP Cytiva NA934-100UL. For IF - 1:500

Validation

All antibodies were prevalidated by manufacturer and prior research, as stated in the supplied antibody data sheet and QA certificate.
Primary antibodies:
1) Anti-total-tau Genetex GTX49353. For IF - 1:750
https://www.citeab.com/antibodies/3843065-gtx49353-tau-antibody?des=37dc0705dd718164
2) Anti-p-tau PHF1 Albert Einstein College of Medicine. For IF - 1:500
Validation for IF - https://www.nature.com/articles/nprot.2015.065
3) Anti-p-tau (AT180) Invitrogen MN1040. For IF - 1:500
Validation for IF based on 15 publications appearing in - https://www.thermofisher.com/antibody/product/Phospho-Tau-Thr231-Antibody-clone-AT180-Monoclonal/MN1040
4) Anti-total tau (Dako) Agilent A0024. For ELISA - 1:10000. For IF - 1:1000
Validation for ELISA and IF based on publications appearing in - https://www.citeab.com/antibodies/3382933-a0024-tau
5) Anti-HSV1-VP21/VP22a (LP13) Invitrogen MA5-16798. For ELISA - 0.04, 0.2, 1.0, 5.0 µg/mL
Validation for ELISA is unavailable - https://www.thermofisher.com/antibody/product/HSV-Type-1-VP21-VP22a-Antibody-clone-LP13-Monoclonal/MA5-16798
6) Anti-HSV1-ICP5 Virusys Corporation HA018-100. For ELISA - 0.04, 0.2, 1.0, 5.0 µg/mL
Validation for ELISA is unavailable - https://www.antibodyregistry.org/AB_2713935
7) Anti-HSV1-pUL25 Homa Lab University of Pittsburgh. For ELISA - 0.04, 0.2, 1.0, 5.0 µg/mL
Validation for ELISA is unavailable
8) Anti-HSV1-pUL48-VP16 Novus Biologicals NB206593. For ELISA - 0.04, 0.2, 1.0, 5.0 µg/mL
Validation for ELISA is unavailable
9) Anti-HSV1-RS1-ICP4 (10F1) Abcam ab6514. For ELISA - 0.04, 0.2, 1.0, 5.0 µg/mL
Validation for ELISA - https://www.abcam.com/en-us/products/primary-antibodies/hsv-1-icp4-immediate-early-protein-antibody-10f1-ab6514?srsltid=AfmBOoqyYUqtntAL0vC1knr7ylmVbVcVK42FRhW3zNLrb02FRO3hQ1Mp
10) Anti-INFγ antibody Invivogen HIFNG-MAB7-02. For neutralization - 10 µg/mL
Validation for neutralization is unavailable
11) Anti-HSV1 (strain 17) Invitrogen PA5-115473. For IF - 1:1000
Validation for IF is unavailable - https://www.thermofisher.com/antibody/product/Herpes-Simplex-Virus-Type-1-strain-17-Antibody-Polyclonal/PA5-115473
12) Anti-IBA1 Abcam ab283346. For IF - 1:1000
Validation for IF - https://www.abcam.com/en-us/products/primary-antibodies/iba1-antibody-epr16589-microglia-marker-rat-igg2a-chimeric-ab283346?srsltid=AfmBOopLuU6otfbOllz4TQhqQbSgOM0TEF39XdxJqM_Vw27-o0Fev279

Eukaryotic cell lines

Policy information about cell lines and Sex and Gender in Research

Cell line source(s)	Niave and genetically modified ReNcell VM human neuronal progenitor cell line - Millipore Sigma. Modified lines produced as previously published. Choi et al 2014 Nature.
Authentication	Modified lines were isolated and identified as previously published. Choi et al 2014 Nature.
Mycoplasma contamination	Mycoplasma Detection Kit from Lonza was used to assess contamination in each cell line. Results were negative.
Commonly misidentified lines (See ICLAC register)	No commonly misidentified lines used.

Plants

Seed stocks	N/A
Novel plant genotypes	N/A
Authentication	N/A